Growth and Characterization of Epitaxial FeCo/MgO/EuS Magnetic Tunnel Junctions on MgO Buffered (100)-Si

by
Zhiwei Gao

A thesis
presented to the University of Waterloo
in fulfillment of the
thesis requirement for the degree of
Master of Applied Science
in
Electrical and Computer Engineering

Waterloo, Ontario, Canada, 2016

AUTHOR'S DECLARATION

I hereby declare that I am the sole author of this thesis. This is a true copy of the thesis, including any required final revisions, as accepted by my examiners.

I understand that my thesis may be made electronically available to the public.

Abstract

In the last few decades, due to the dramatic improvement of the TMR (tunneling magnetoresistance) effect in MTJs (Magnetic Tunnel Junctions), the data storage industry has been revolutionized. There are so many applications based on this technology, e.g.: read head in hard disk drives; magnetic sensors, etc., while its most advanced application nowadays is on the Magnetoresistive Random Access Memory (MRAM), a type of nonvolatile, high speed, high density, yet low power consumption memory - often termed the "universal memory" [1].

For most applications, magnetic tunnel junctions are fabricated with thin film technologies. In industry, they are mostly deposited by magnetron sputtering for mass production purposes. While in research laboratories, MBE (Molecular Beam Epitaxy), PLD (Pulsed Laser Deposition), and E-beam (Electron beam physical vapor deposition) are often used to deposit well-controlled, high quality layers.

The very core component of an MRAM cell is an MTJ, which possesses the desired TMR effect. An MTJ basically consists two ferromagnetic materials separated by a thin insulator. Typically, the connection across the insulating layer is what we call a junction, and the layer is usually a few nanometers thick, which ensures that the junction is thin enough to let the electrons tunnel from one side of the insulator to the other. This is a purely quantum mechanical phenomenon and will be forbidden in classical physics because classically an insulator cannot conduct.

In this thesis, we demonstrated the epitaxial growth of the tunnel junctions FeCo/MgO/EuS/Ti on MgO-buffered Si (100) wafers, and showed that TMR in these junction reaches up to 64% at 4.2K. We also discovered how different thicknesses of MgO and measurement temperatures affect the TMR of these junctions. We then optimized the growth conditions of the junctions, and used XPS (X-Ray Photoelectron Spectroscopy) to analyze their chemical characteristic features. The best TMR occurring at 1nm MgO thickness is a result of the competition between symmetry enhancement through MgO, and thickness induced multistep hopping.

Acknowledgements

The author would like to thank Prof. Guo-Xing Miao for his supervision, and Qian Xue, Yongchao Tang, Yuantao Ji, Hui Zhang, Lin Li, and Yihang Yang for their collaborations. The author would also like to thank Prof. David Cory and his team members for their assistance on this project, and Prof. Manoj Sachdev for his review and comments on this thesis.

Table of Contents

List of Figures

Chapter 1
Introduction

1.1 Motivation

In the last twenty years, due to the dramatic improvement of the TMR (tunneling magnetoresistance) effect in MTJs (Magnetic Tunnel Junctions), the data storage industry has witnessed an exponential expansion. There are so many applications based on this technology, e.g.: read head in hard disk drives; magnetic sensors, etc., while its most advanced application nowadays is on the Magnetoresistive Random Access Memory (MRAM), a type of nonvolatile, high speed, high density, yet low power consumption memory - often termed the “universal memory” [1].

MRAM is a nonvolatile random-access memory technology under development since the 1990s, whose core components are made of MTJs. Continued increases in density and reduction in cost of existing memory technologies – notably flash RAM and DRAM – pushes MRAM in a niche role on the market, but its durability and low power consumption render it irreplaceable in some extremely demanding applications, such as on satellites or for field deployment. Unlike conventional RAM chip technologies, data in MRAM are not stored as electric charges or current flow, but as relative magnetic orientations between the magnetic storage elements. Each storage unit is formed with two ferromagnetic layers separated by a thin insulating layer, in other words, an MTJ. One of the two layers is pinned to a particular direction through exchange bias; the other one's magnetization can be changed with an external field (or a spin current) to write or erase the memory state. This configuration is the basic structure for an MRAM bit. A memory device is built from a grid of such "cells"(Figure 1-1).

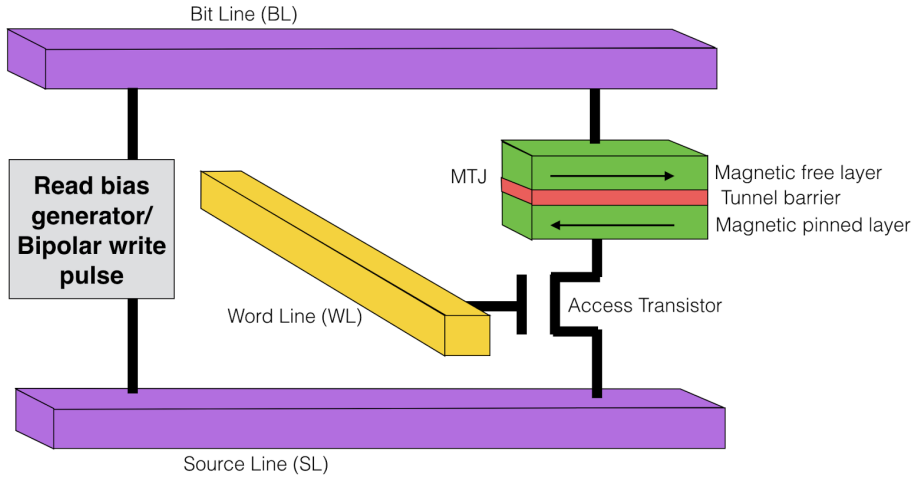

Figure 1-1 Schematics of a memory cell of the STT (spin-transfer-torque) MRAM. Unlike DRAM, MRAM uses resistance-based storage instead of voltage-based. Changing the resistance of the MTJ leads to changing the data. To read the data, we could add a small voltage between the bit and source line, and the current is sensed. To write the data, we could add a large voltage to have a large amount of current push through the MTJ and change the free layer magnetization through spin-transfer-torque. The writing current polarity determines the written data bit. If the orientation of the free layer is the same as the fixed layer, ie., a parallel configuration, it is stored as logic 0; if anti-parallel, it is stored as logic 1. Both read and write operation mentioned above are activated with the word line by controlling the transistor.

The performance of the current DRAM technologies is limited, because the speed at which the charges stored in the cells that can be drained (erasing data) or stored (writing data) is slow, not to mention the large energy overhead associated. As a comparison, MRAM, especially STT-MRAM, is a new kind of technology that benefits from the intrinsic spin dynamics for rewriting the data, which has a much shorter and well controllable settling time. In addition, it does not require constant refreshing the data bits, therefore dramatically increasing its energy efficiency. Researchers in IBM have already demonstrated that the access time of MRAM can be reduced to the order of several nanoseconds, while the enhanced and newest DRAM devices do not come close to it [2]. In Germany, PTB team (Physikalish-Technische Bundesanstalt) further reduced the settling time to only one nanosecond, way better than the theoretical limits of DRAM [3]. When compared with flash memory,

another type of popular nonvolatile memory, the write speed of MRAM is thousands of times faster, and the write-erase durability is millions of times better [4].

As we mentioned before, MRAM is made of MTJs, which have a magnetoresistance response called TMR. An MTJ basically consists two ferromagnetic materials separated by a thin insulator (Figure 1-2). Typically, such a connection across the insulating layer is what we call a tunnel junction, and the insulator barrier is usually a few nanometers thick, which ensures that the junction allows the electrons to tunnel from one side of the tunnel barrier to the other. This is a quantum mechanical phenomenon and is forbidden in the classical world. Classically one would expect that electrons cannot pass through an insulator.

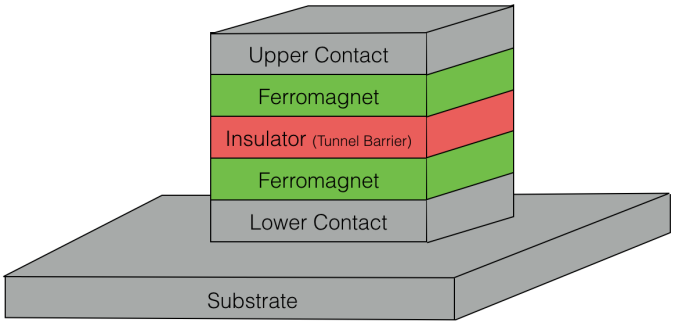

Figure 1-2 MRAM is made of MTJs, which are basically two ferromagnetic materials separated by a thin insulator. They show a strong magnetoresistance effect called Tunnel magnetoresistance

In 1975, M. Jullière first discovered the TMR effect in University of Rennes, France. The junction was Fe/Ge-O/Co measured at a low temperature of 4.2K. The TMR was 14%, but it did not generate much attention in the academic world due to the low operation temperature [5]. 16 years later, Terunobu Miyazaki found a 2.7% TMR at room temperature in Tohoku University, Japan, and later improved it to 18% for Fe/Al2O3/Fe [6]. At the same time, Jagadeesh Moodera in Massachusetts Institute of Technology found 11.8% TMR at room temperature with electrodes of FeCo and Co [7]. Since 2000, epitaxial MgO has become the most popular tunnel barrier choice. In 2001, Butler and Mathon both predicted that (100) epitaxial iron is a ferromagnetic material matching (100) MgO, and together they can theoretically boost the TMR ratio to thousands percent [8,9]. Just three years later,

Parkin and Yuasa made CoFeB/MgO/CoFeB and Fe/MgO/Fe junctions respectively, and reached >200% TMR at room temperature [10, 11]. In 2008, Ohno group in Tohoku University, Japan, achieved TMR of 1100% at 4.2K and 600% at RT in CoFeB/MgO/CoFeB tunnel junctions [12].

Magnetic tunnel junctions are fabricated by using thin film technologies. In industry, they are deposited by magnetron sputtering for mass production. While in research laboratories, MBE (Molecular Beam Epitaxy), PLD (Pulsed Laser Deposition), and E-beam (Electron beam physical vapor deposition) are mostly used to deposit the layers. For example, the CoFeB/MgO/CoFeB junctions mentioned above were made by sputtering, while the Fe/MgO/Fe ones are by MBE. Post annealing is critical for the former process, while suitable temperatures are directly applied to each deposition step in the latter.

Choosing correct materials seems the most important thing to achieve better TMR. Large TMR leads to stronger signals in actual data storage devices. In order to have a decent TMR effect, the barrier layer ideally should have a rock-salt structure; additionally, the crystal lattice of the material should match that of Fe or FeCo to enhance the coherent Bloch state tunneling. MgO is so far the most popular tunnel barrier material with lots of successful achievements, so we also choose MgO to be part of the tunnel barrier. In addition, we also incorporate EuS as a spin filter layer, whereas nonmagnetic Ti as the top electrode instead of using another ferromagnetic layer. EuS is a material with a rock salt lattice structure and lattice-matched with MgO. Europium and Sulfur atoms both form fcc (face-centered cubic) crystal lattice and have octahedral coordination geometry with each other. The lattice constant of EuS is 5.968 Å. The crystal structure of EuS is shown in Figure 1-3.

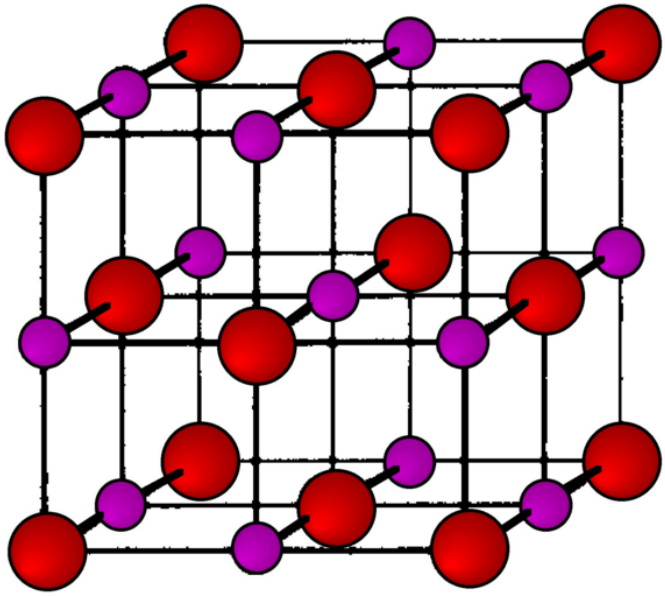

Figure 1-3 EuS is a material with a rock-salt lattice structure. Europium and Sulfur atoms form octahedral coordination geometry with each other. The lattice constant of EuS is 5.968 Å, matching that of MgO within 0.2% [13]

Theoretically, there are 4 kinds of Bloch states most relevant to the bcc (body-centered-cubic) structured electrodes (such as the Fe and FeCo we used), they are termed the Δ1, Δ2, Δ2', and Δ5 states, as you can see in Figure 1-4. For these four states, each has a different decay rate with the distance it travels inside the tunnel barrier. In an epitaxial bcc-Fe/MgO/bcc-Fe system, the one with the slowest decay rate, Δ1 state, plays the most important role as electrons of this state are least attenuated when tunnel through the barrier, and they are also completely spin-polarized from the Fe bands. For Δ5 electrons, some of them are spin-polarized but some are not, fortunately most of them will be filtered out as the MgO thickness increases. This is the reason why TMR generally gets higher with increasing MgO thickness, because the undesired states (such as Δ5) are effectively filtered out with thickness. The least contribution one is Δ2', which fades away almost instantly.

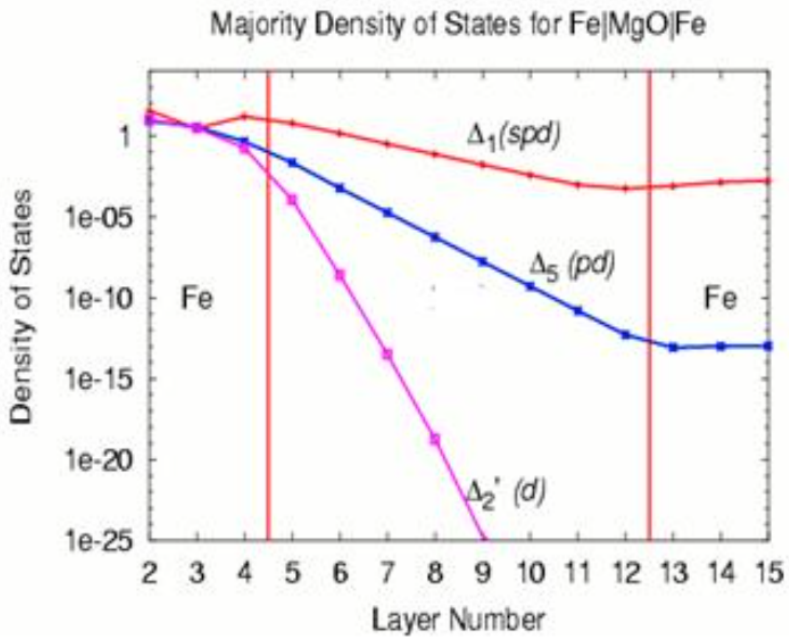

Figure 1-4 There are 4 kinds of Bloch states most relevant to the TMR effect in Fe/MgO/Fe, they are Δ1, Δ2, Δ2', and Δ5 states and decay at different rates inside MgO [9]

Because the crystal structure of Europium Sulfide is fairly similar to that of magnesium oxide [14, 15 16], we could get epitaxial EuS at suitable growth temperatures on epitaxial MgO. Epitaxial MgO has been achieved from our previous experience. For this reason, we also get fairly good coherent tunneling [8,17,18,19,20,22], although the coherence seems to vanish faster than we had anticipated.

In this thesis, we report the deposition of hybrid Magnetic Tunnel Junctions of Fe/MgO/EuS/Ti, ie., combining epitaxial MgO and spin filter, and discuss their interesting results.

1.2 Objective

In this thesis, we will demonstrate and optimize TMR of the junctions Fe/MgO/EuS/Ti at low temperature of 4.2K. We want to find out the trend how different thicknesses of MgO and

measurement temperatures affect the TMR, paving roads for potentially constructing devices with better performance. We also use XRD and XPS to analyze the structural and chemical characteristic features of the junctions, in order to optimize the growth conditions of the junctions.

1.3 Structure

In Chapter 2, we will introduce to the readers the background knowledge, which covers MTJ (Magnetic Tunnel Junction), TMR (Tunneling magnetoresistance), and spintronics.

In Chapter 3, we will go through some experiments that were previously performed by our or other groups related to the growth of EuS and MgO junctions.

In Chapter 4, we explain in details the experimental process and methodology of the deposition, creation, and measurement of the whole junction structures that we used.

After illustration of the fabrication processes of the junctions, we further discuss the results of our experiments in Chapter 5.

Finally, we propose some future works for further improving the performance in Chapter 6.

Chapter 2
Background

In this chapter, we will introduce to you the background knowledge of MTJ (Magnetic Tunnel Junction), TMR (Tunneling Magnetoresistance), and spintronics.

2.1 Spintronics

In terms of solid-state electronic devices, electron charge flow and storage always play the most important role. On the other hand, each electron also carries a spin with it, which can be harvested for additional information processing. Integrating the fundamental electron charges and spins into a single device, namely a spintronic device, is the future of the solid-state devices towards higher integration and lower power consumption.

Spintronics is still a relatively young field. Spin-dependent electron transport has just been demonstrated for four decades, as we mentioned in the introduction part, GMR (giant magnetoresistance) and tunneling magnetoresistance are discovered in 1988 and 1970s, respectively. The mass application of spintronic devices only started in 1997 with the first GMR based hard disk drive (HDD) deployed by IBM.

There are two main components in the angular momentum, the first one is the orbital angular momentum, and the other one the spin angular momentum. For the orbital angular momentum, it is generated by motion of the charged electrons; but for the spin angular momentum, it comes from the intrinsic spin of the electrons. Because 1/2 is the spin quantum number of an electron, the projection of the spin angular momentum in any direction is always 0.5ħ. And because this spin quantum number is a half-integer, electrons are classified as fermions [40]. Both of the angular momenta mentioned above generate magnetic moments. The magnetic moment generated by the spin angular momentum is shown below. In any given arbitrary direction, the projection of the electron moment is one Bohr magneton μ_B.

$$\mu = \frac{\sqrt{3}}{2}\frac{q}{m_e}\hbar$$

If the electron spins are correlated, they can change the electronic and magnetic features of the material; for example, they may transfer the material into a ferromagnet that has spontaneous magnetic moments. For most materials, the quantity of spin-up and spin-down electrons are the same, therefore, they appear nonmagnetic. However, we could use spintronics to change, or shall we say, manipulate the spins of the electrons to perform information processing. The spin polarization that we defined earlier is shown below, where X is the dependent property.

$$P_X = \frac{X_\uparrow - X_\downarrow}{X_\uparrow + X_\downarrow}$$

As to be discussed later, we could create a splitting of band heights on the two spin channels, then we would have different amount of spin-up and spin-down electrons in the transport. Similar to the Zeeman effect under magnetic fields, we could easily use a magnetic insulator to induce a huge magnetic exchange field onto a material, which will generate an extremely strong Zeeman splitting [41,42,43]. Another example is spin pumping, which is a method that can generate spin current via collective spin precession [30,45,47]. The time to maintain a non-equilibrium spin is the spin lifetime. Nowadays, scientists are trying hard to increase the spin lifetime for easy manipulation. Decay of spin signals has several mechanisms, and most of them are related to dephasing and spin-flip scattering [48,49,50]. Selecting suitable materials can to a large extent reduce such undesired spin signal loss.

2.2 Magnetic Tunnel Junctions

There are three core elements in a standard MTJ, the order from bottom to top are: bottom electrode, tunnel barrier, top electrode. The bottom and top electrodes are made of ferromagnetic materials. The layer sandwiched by the electrodes is the tunnel barrier. This tunnel layer is made of dielectric materials, and only a few nanometers thick (Figure 2-1).

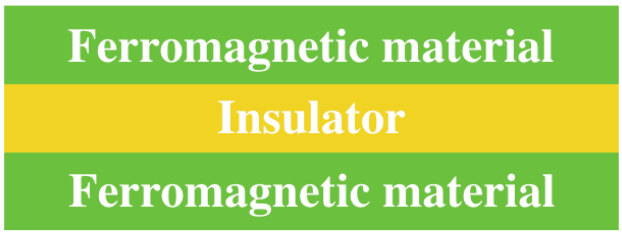

Figure 2-1 The structure of an MTJ (Magnetic Tunnel Junction)

Usually, Magnetic tunnel junctions are fabricated with thin film technologies. In industry, they are mostly fabricated by magnetron sputtering due to the need of mass production. While in laboratories, MBE (Molecular Beam Epitaxy), PLD (Pulsed Laser Deposition), and E-beam (Electron beam physical vapor deposition) are often used to deposit the layers for better control and material quality. In this thesis, the junction deposition is achieved in a high vacuum electron-beam deposition system.

2.3 Tunneling Magnetoresistance

The Tunneling Magnetoresistance is an effect that occurs in the magnetic tunnel junctions. We apply an external field to the junction, which can control the magnetic directions of the top and bottom layers independently. When the orientations of the spins in the two ferromagnetic layers are parallel, the electrons will easily tunnel through the tunnel barrier; but tunneling is not as easy when the magnetic orientations are antiparallel. Hence, we could get two stable resistance states in the magnetic tunnel junction, low or high. This resistance change with field is the tunneling magnetoresistance effect we are interested in (Figure 2-2).

The TMR ratio is the ratio of the resistance change over the parallel state resistance.

$$TMR = \frac{R_{ap} - R_p}{R_p}$$

Where R_{ap} is the resistance of the magnetic tunnel junction when the spin configuration is anti-parallel, and R_p is the resistance when the spin configuration is parallel.

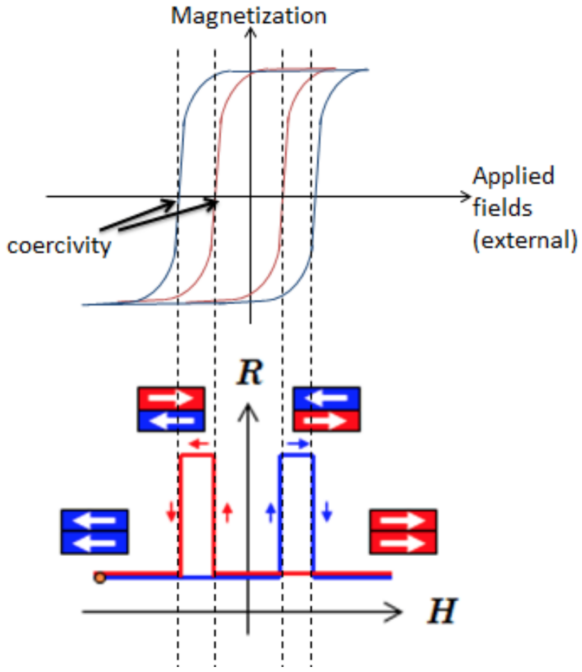

Figure 2-2 The upper figure shows the hysteresis loops of the two ferromagnetic materials. A hysteresis loop gives you the detailed information of how an external field affects the magnetization of the material. The field when the magnetization reverses sign is called the coercive field, and it will be sensitively affected by the thickness of the ferromagnetic material. The bottom figure shows that when the two materials' coercive fields are different, antiparallel states will be achieved over a certain field window [26]

With defining a spin polarization of ferromagnetic materials, M. Jullière first quantified the TMR effect. The spin-dependent DOS (density of states) determines the spin polarization of the electrodes. The relationship between the DOS and spin polarization P is shown below,

$$P = \frac{D_{\uparrow}(E_f) - D_{\downarrow}(E_f)}{D_{\uparrow}(E_f) + D_{\downarrow}(E_f)}$$

For electrons, their spins can have two states: when their spin orientations are in the same direction as the magnetization, the electrons are in the spin-up (spin-majority) states; when they are opposite, the electrons are in the spin-down (spin-minority) states. If P_1 and P_2 are the spin

polarization of the two ferromagnetic materials, the TMR ratio can be written as the following equation:

$$TMR = \frac{2P_1P_2}{1 - P_1P_2}$$

The prerequisite of TMR is that the electrons should be able to tunnel through the magnetic tunnel barrier while maintaining their spin coherence (Figure 2-3a). The current can be divided into two separate channels, the spin-up and spin-down currents, and they flow independently. The magnetic state of the Magnetic tunnel junction determines the conductance of these two channels [23,24]. For most MTJs, with increasing temperature and increasing bias voltage, the TMR decreases due to increased spin-flipping. As you can see, TMR will in principle be infinite when the magnetic electrodes' spin polarizations are both 100%, ie., both are half-metals [25].

TMR has another important means for enhancement, which is called symmetry filtering. The tunneling matrices are not the same when the incoming electrons have different Bloch wave states, in other words, the barrier is not merely an energy barrier and it has its preferred symmetry. Because of this, the most famous development in this field - magnesium oxide sandwiched by iron, was predicted theoretically and demonstrated experimentally with giant TMR much larger than that expected from Julliere's model [8,9,11,10]. As one can see below, the symmetry filtering further imposes wavefunction coherence, and plays an important role on spin selectivity for improving the TMR.

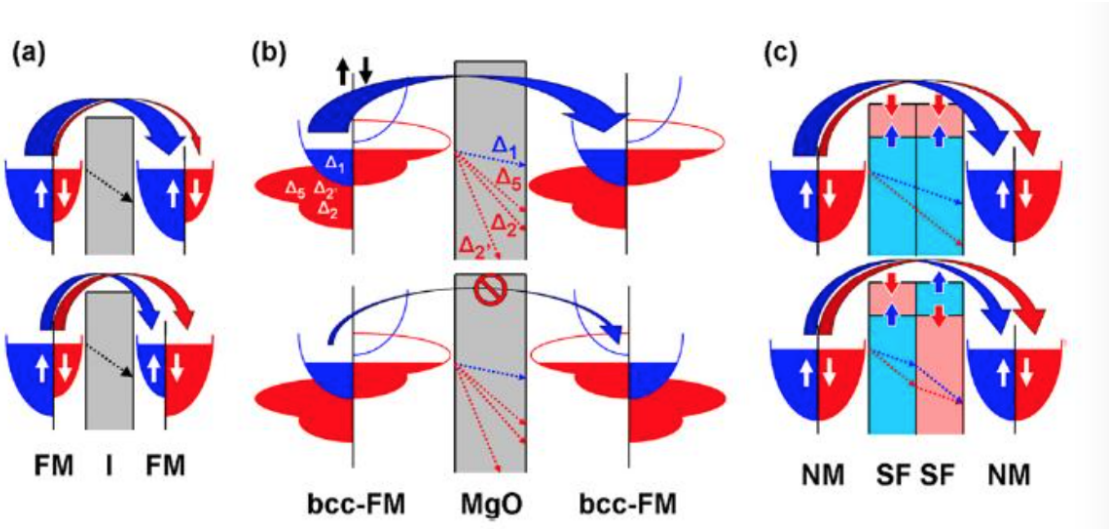

Figure 2-3 The principles of TMR. Upper diagrams are for the parallel states and the lower diagrams are for the antiparallel states. For (a), a conventional energy barrier is shown, as you can see in the graph, the decay rates of the tunnel electrons are the same regardless of spins. TMR is mainly determined by the DOS of electrodes, the more electrons are spin polarized, the higher TMR they generate. For (b), It is what we call a symmetry filtering barrier. The decay rates are different for electrons in different Bloch states. The Δ1 state obviously has the slowest decay rate in the Fe/MgO/Fe epitaxial junction and dominates the transport process. For (c), the diagram is for a spin filter barrier. As one can see, the electrons themselves do not have spin polarization, but the barrier does have spin dependent heights, so that some of the electrons are filtered inside the barrier [10].

As we can see in figure 2-3(b), with the corresponding decay rates shown in figure 1-4, electrons in the Δ1 state have the lowest decay rate inside (100)-MgO, and they are completely spin polarized. This is because Fe does not have Δ1 electrons in the minority spin channels. For magnesium oxide, only electrons in the Δ1 states can easily tunnel through the junction and enter the counter electrode if the junction is in the parallel alignment, resulting in a low junction resistance. But there will be no available states in the counter electrode if the junction is in the antiparallel alignment, and a high junction resistance occurs. This is the reason why the TMR of MgO-based junction is large. The reason that the TMR is not infinite is due to the existence of the undesired states such as Δ5, which generate some conductance even in the antiparallel alignment.

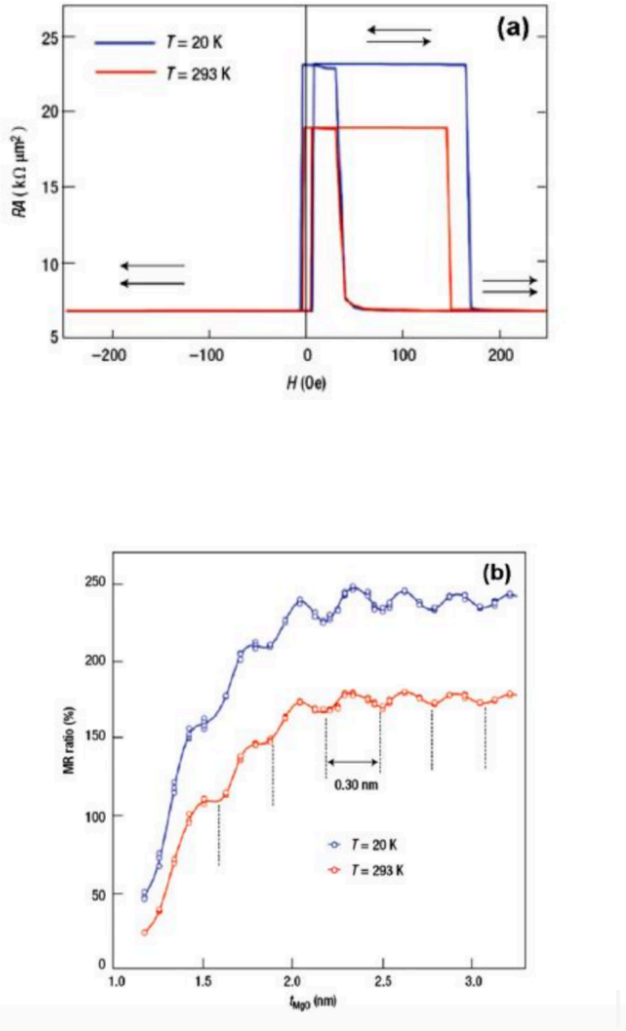

Figure 2-4 Behavior of magnetic tunnel junction Fe/MgO/Fe (a) MR curve and (b) MR vs MgO thickness [10]

Obviously, TMR of the junction is dependent on the thickness of the tunnel barrier, because the filtering (decay of undesired states) is an exponential function on thickness. As you can see, TMR increases with the barrier thickness when the thickness is less than 2nm. Beyond 2nm, TMR is limited by defect-mediated multistep tunneling processes. The Nancy University group showed that epitaxial Cr insertion behaves as a metallic barrier [31], because there are no $\Delta 1$ states in Cr at the Fermi level. Quantum oscillations with Cr layer thickness were also reported by Yuasa group [27]. There are other

ways we could use to modulate the TMR of the junctions as well, for example, we could improve the crystal quality as much as possible to enhance the coherence [32].

There also have been some experiments on dual-barrier junctions taking advantage of the tunneling coherence. By doing this, dual-MgO layer will form a quantum well state in the magnetic tunnel junction [33]. The magnetic tunnel conductance clearly reveals quantum oscillations with regard to the applied bias voltages. Similarly, Fe quantum well insertion between Cr and MgO also shows the TMR and conductance oscillations [34,35]. This is because Cr has no Δ1 states near the Fermi level, therefore it behaves more like a barrier for the dominant electrons.

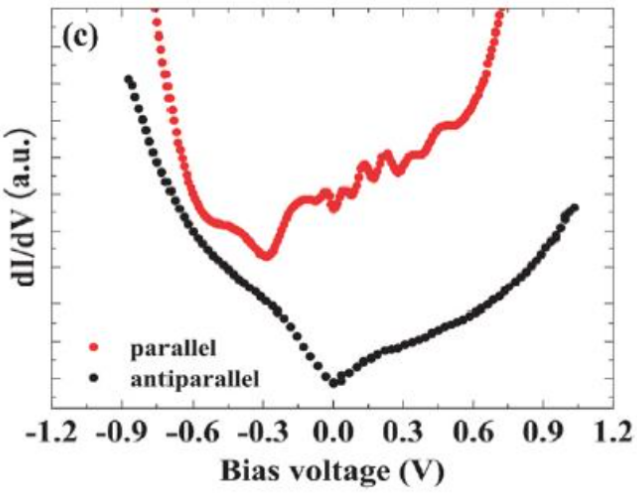

Figure 2-5 The conductance of parallel and antiparallel states in a dual-barrier MTJ: 50nm Fe/2nm MgO/1.5nm Fe/2nm MgO/15nm Fe [33]

We do have yet other ways that can increase the TMR in the MTJs. For examples, we could consider using amorphous electrodes to enhance the interface smoothness [37]. We could also consider optimizing the growth condition of the layers, such as the growth speed and temperature etc. However, the coherence between the magnetic tunnel barrier and magnetic electrode is very important, so we need to make sure that their interfaces are epitaxial. In addition, we could do post annealing after deposition for improving the materials and interfaces, which also enhances the TMR. The surface sensitivity of tunneling creates some of the biggest challenges for the processing. The

very first few atomic layers dominate the effect of the spin tunneling process. We also need to consider the oxidation of the bottom electrodes. In our experiment, we use FeCo to be the bottom electrode; it is possible to become FeO/CoO at the interface between the oxide barrier and the electrode, which will scatter the desired conductance of the $\Delta 1$ bands. Based on our previous experience [38], we used Mg-insertion to solve this problem, and this thin Mg layer will absorb oxygen and also become MgO as part of the junction. In this work, we made a comparison experiment between using and not using the Mg-insertion method in our fabrication process, the result shows that the one using Mg-insertion method has lower TMR by around 10% on 5.5nm FeCo/1nm MgO/3nm EuS/ 10nm Ti junction. Because we did not find any improvement with Mg-insertion in this experiment, it was not used for other samples in this thesis.

Spin filter is another way that can be used to generate spin polarization, and the junctions are called spin filter tunnel junctions, which can also create TMR based solely on spin filtering effect. The spin polarization results from the unequal probabilities of the electrons tunneling through the junction. Figure 2.5 shows the principle idea of the spin filtering. A magnetic insulating material has spin-split barrier heights, which leads to the different tunneling probabilities for the spin up and down electrons. The minority electrons facing the tall barrier will be filtered out [39].

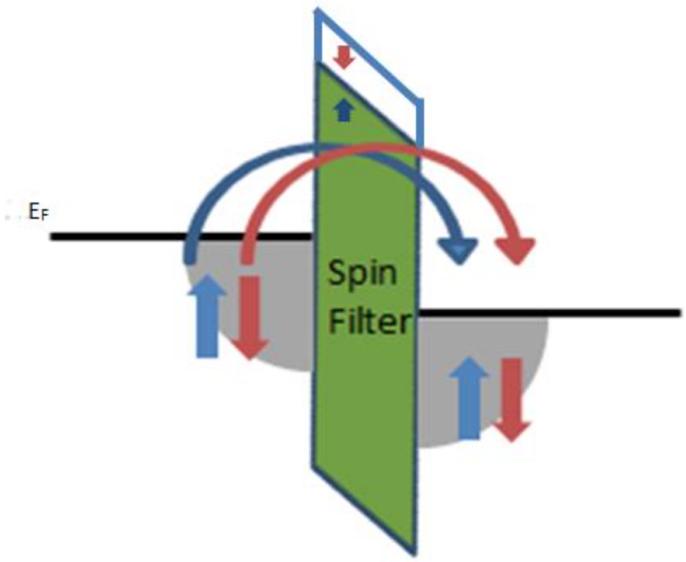

Figure 2-6 Schematics of the spin filtering effect. The middle green block stands for the spin-up barrier height, and blue for spin-down. Blue and red arrows stand for the spin up and down conduction channels, with the spin-up electrons (blue) facing a lower tunnel barrier height and higher tunnel probability [39].

2.4 Spintronics Applications

TMR devices are already widely used in industries, for example, in making read heads in hard disk drives. The advantage of using TMR is that it could even read out data from a HDD storage media with density more than 500GB/inch^2. The storage unit is still getting more compact and faster because of the better TMR and faster switching speed.

We can also use the TMR technology on magnetic sensors, as well as spin-logic units and nonvolatile memory devices. For nonvolatile memory devices, the most famous development is called MRAM (Magnetoresistive Random Access Memory), which has already been deployed in many industry sectors. The basic principle is that the TMR can convert the direction of the magnetization into a resistance reading. This leads to the major advantages of using MRAM rather than DRAM: MRAM is nonvolatile and retains its data without consuming power, because the data are reliably stored as the magnetization directions. In addition, MRAM has almost the same speed and density as

DRAM. Because of the nonvolatile nature, MRAM do not need to regularly refresh the data so it has better performance and is much more efficient in terms of energy consumption.

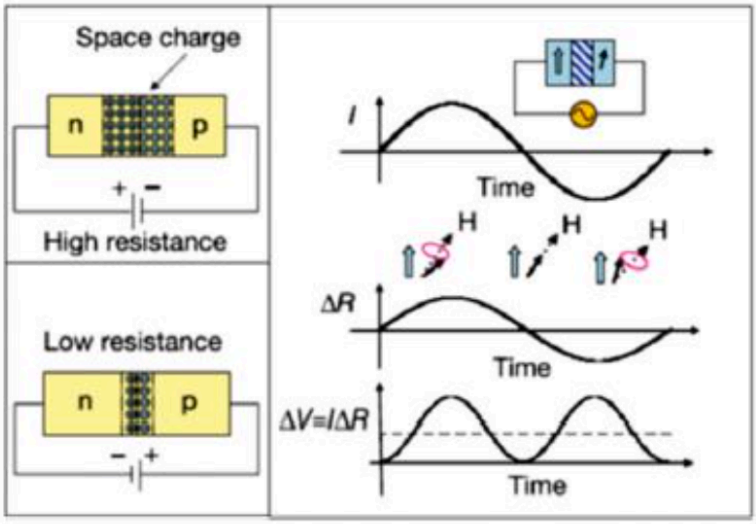

Figure 2-7 This is the schematic comparison of a spin-torque diode and a p-n junction. As we can see on the diagram, changing the voltage can change the depletion layer thickness in a regular diode and therefore change its impedance. In a spin-torque diode, the magnetic layer precession is synced with the driving spin-torque current, and a DC voltage is produced as a result of the oscillating current and junction impedance together [54].

Spin-polarized current can affect the orientation of the magnetic layer of the MTJ, this is what we call the spin-transfer torque [53]. When the TMR is sufficiently large, the spin-torque diode (Figure 2-7) functions as a regular ON/OFF diode. Additionally, when the free layer of an MTJ is driven near its intrinsic FMR frequency, the orientation of the electrons will rotate with the applied AC current. During the first half of the voltage cycle, the angle between the free layer and the fixed layer is getting larger and larger, while the second half smaller and smaller. So the device resistance is getting larger in the first half but getting smaller in the second half, and multiplied with the AC current, we then have a DC voltage output by using an AC current as the input [54].

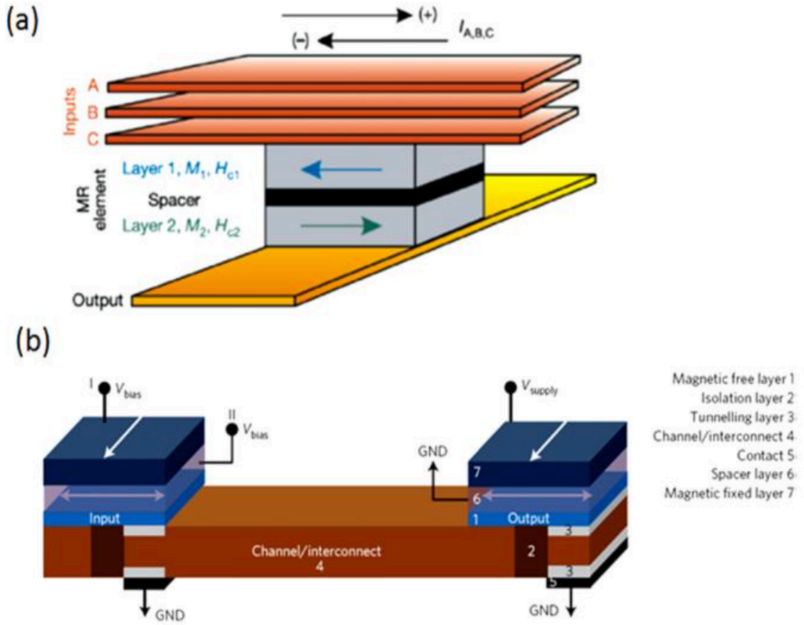

Figure 2-8. Two types of spin logic TMR devices. The upper one is a programmable spin logic unit. The lower one is an all-spin-logic-device [51, 52].

We listed two kinds of spin logic devices on figure 2-8, the upper panel is a programmable logic device. This type of device can be used to create reprogramming computing ships. The high and low resistances are being defined as 0 and 1. The 'plus' and 'minus' computing operators are defined as manipulating the orientation of the magnetization in one of the magnetic layers (either M1 or M2) while fixing the other one.

The lower panel is the all-spin-logic-device (ASLD), unlike the scenario of the programmable spin logic unit, which fixes one magnetization and changes the other, ALSD is using spin current addition and subtraction to perform the computing operations. The device has many equivalent units, and each of them can create a spin current as the output, or take the spin current as the input. If a large supply voltage is added from the top across the fixed layer 7, due to the spin-transfer-torque effect, the free layer 1 will be driven to the neutral position. Now if we turn off the supply voltage, the spin current flowing in channel 4 from the previous unit can determine the final magnetization direction, ie., rewriting the bit state. One of the advantages of the ALSD is that it has its own built-in memory function, so it will have better performance than regular CMOS based devices [52].

Chapter 3
Literature Review

For this chapter, we will go through some experiments previously done by our or other groups that are related to this thesis work.

3.1 Magnetic Properties of EuS

The magnetic properties of EuS have been well studied in the 1960s by several researchers around the same time [55,56,57]. EuS is a ferromagnetic insulating material, and its Curie temperature is between 15K and 16K, the transition temperature determined from specific heat measurement is 16.3K [58].

Busch et al measured its band gap in details [59]. The gap is 1.645eV at room temperature. There is a negative temperature coefficient of 1.7×10^{-4} eV/degree in the paramagnetic region.

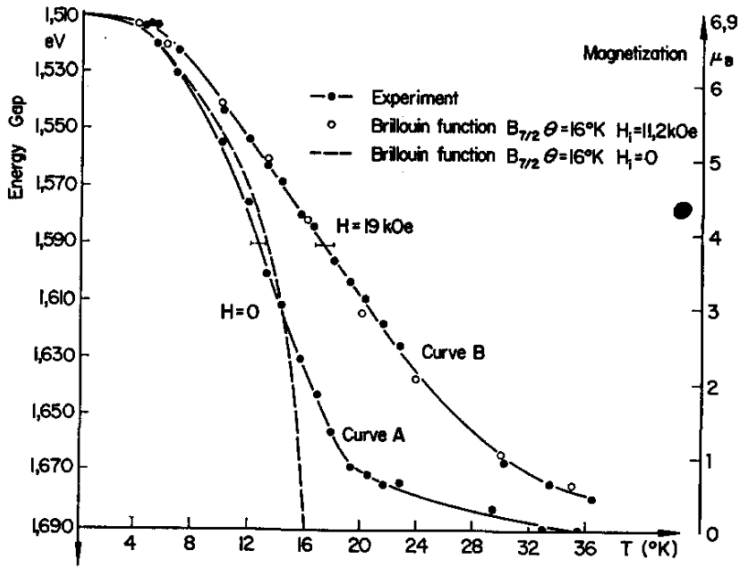

Figure 3-1 The absorption edge (band gap) changes with temperature [61]. The left y-axis shows the energy gap, which are measured from the experiments. The dashed line and the open circles are theoretical results of magnetization (right axis) when the internal magnetic field H_i is 0 kOe and 11.2 kOe, respectively. The two solid lines (with closed circles) are the experimental results

when the external magnetic fields are 0 kOe and 19 kOe respectively. Because the experimental results well match the Magnetization of EuS calculated using the Brillouin's function M(H_i, T), it was concluded that the Magnetization is a linear function of the absorption edge shift.

As one can see in Figure 3-1, the position of the absorption edge changes with temperature. The energy gap decreases from 1.69 eV to 1.51 eV when the temperature cools down from 36K to 2.3K.

From Figure 3-1, we also notice that the magnetization varies when the temperature is changed. The magnetization of EuS has also been plotted in the same temperature range. They used the expected saturation magnetization of 6.8 μ_B to tune the maximum shift of the absorption edge by extrapolation to 0K. The magnetization M has been calculated using the Brillouin's function, and shows that M is a function of two factors: the internal magnetic field Hi, and the temperature. The calculated results are compared with the experimental results (the shift of absorption edge by applying 19 kOe Magnetic field). From the fitting it was concluded that the shift of absorption edge is a linear function of magnetization. The spontaneous magnetization is also calculated and plotted [61].

3.2 Spin Filter Effect of EuS Tunnel Barriers

Spin-polarized tunneling is first discovered in the Zeeman-split quasiparticle density of states of superconductors. From the early studies of spin-polarized tunneling, it was confirmed that different densities of spin-up and spin-down electrons at the Fermi level of the electrodes lead to the spin polarization of the tunnel current. [61]. Later on, the researchers used a kind of ferromagnetic insulator as the tunnel barrier, such as EuS [62, 63]. The conduction band of EuS is split into spin up and spin down sub-bands below its Curie temperature, which will lead to different barrier heights for the two spin channels. As a result, electrons with different spin orientations will tunnel with different probabilities and induce a net spin polarization in the tunnel current.

When we use EuS as the tunnel barrier, the barrier heights of spin up and spin down electrons are affected by the conduction band splitting of EuS.

$$\phi_{\uparrow,\downarrow} = \phi_0 \mp \Delta E_{ex}(T)/2$$

In which ϕ_0 is the average barrier height when the temperature is greater than the Curie temperature. Because quantum tunneling is very sensitive to the changing of the barrier height, the splitting of conduction band in EuS will increase the tunneling probability of spin up electrons and decrease that of the spin down electrons. The spin filter effect is shown in Figure 3-2. Large spin polarization of P = 89±7% was demonstrated by means of field emission from EuS-coated tungsten tips [64, 65].

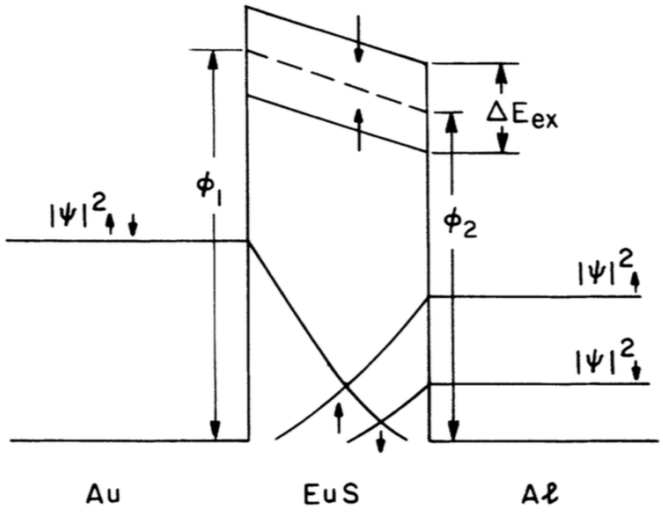

Figure 3-2 Schematics of the spin filter effect. When the temperature is above the Curie temperature, the tunnel barrier height is indicated with the dashed line, while the solid lines are for barrier heights of the spin up and spin down channels below the Curie temperature. The spin up and spin down tunnel probabilities are illustrated as the decay of the wave functions amplitudes [60].

In 1988, Moodera et al in the Francis Bitter Magnet Laboratory at MIT first observed the spin-filter effect of EuS in a superconductor tunnel junction (Au/EuS/Al) [66]. They demonstrated over 85% electron-spin polarization in the tunnel current [60]. As you can see in Figure 3-3, the conductance curves vary with the external magnetic fields on the junction of 11nm Au/ 3.3nm EuS/ 4.2nm Al. The spin polarization can be deduced from the asymmetry of the conductance curves.

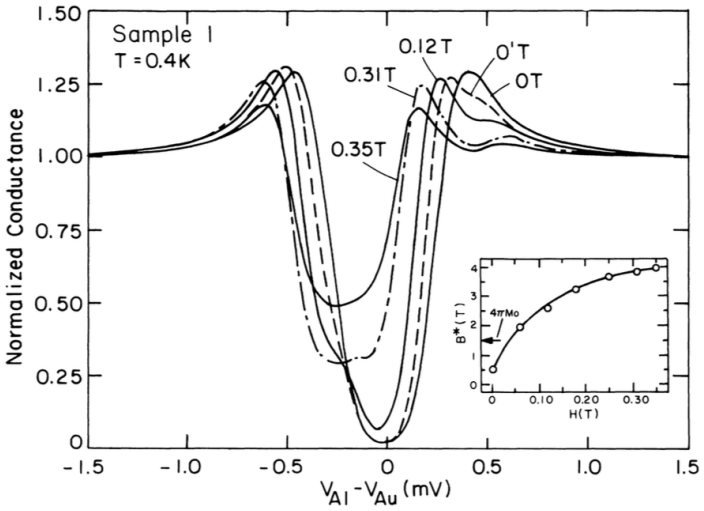

Figure 3-3 The dynamic conductance (*) under different external magnetic fields on a junction 11nm Au/ 3.3nm EuS/ 4.2nm Al. The internal fields ($\boldsymbol{B_i^*}$) can be easily deduced by fitting the curves with the theoretical calculation. The bottom right insert shows the relationship between the effective internal fields and the applied external magnetic fields. We can determine the zero-field $\boldsymbol{B_i^*}$ from the curve at 0T, which shows 0.5 T. We can also find the Remnant Zeeman splitting (curve 0'T) where $\boldsymbol{B_i^*}$ is equal to 2.0T. The arrow stands for the saturation magnetization of EuS, at 1.5T = $4\boldsymbol{\pi M_0}$ [66]. (*) Dynamic conductance: $(\frac{\boldsymbol{dI}}{\boldsymbol{dV_{SN}}})/(\frac{\boldsymbol{dI}}{\boldsymbol{dV_{NN}}})$.

They also tried to use V and V-Ti alloy as the electrodes. The junctions Ag/ 10nm EuS/ 10nm V/ 1.5nm Al and Ag/ 10nm EuS/ 10nm VTi/ 1.5nm Al were fabricated [66]. The spin polarized tunnel conductance is shown on Figure 3-4, and the clear asymmetry indicates a spin polarized current flows across the barrier.

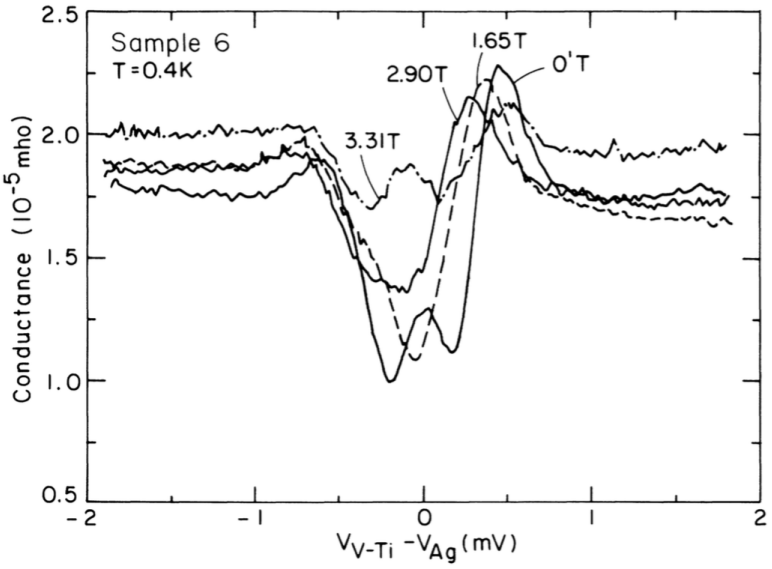

Figure 3-4 The conductance curves for a junction Ag/ 10nm EuS/ 10nm VTi/ 1.5nm Al under different external magnetic fields [66].

3.3 Single and Double Spin Filter(s) Tunnel Junctions

As far as we know, there are no reported works using EuS coupled with MgO. However, there was a nice experiment which used a similar spin-filter tunnel barrier material EuO. The junctions were fabricated using MBE and the achieved TMR was as high as 40% at 1K [67]. Later on two EuS layers were combined to build double spin filter junctions with Al electrodes, and the TMR reached 60% [68]. We will discuss more about these papers because the mechanisms are similar to the work of this thesis.

EuO is a ferromagnetic insulator, and its Curie temperature is 69K. The samples were fabricated under different oxygen pressure mixed with the same Eu flux [67]. The magnetic properties of EuO have been studied in detail. In Figure 3-5, as you can see, the best magnetic moment achieved was around $6\mu_B$/Eu, with the growing oxygen pressure around 4×10^{-8} torr. Its Curie temperature is very close to 69K.

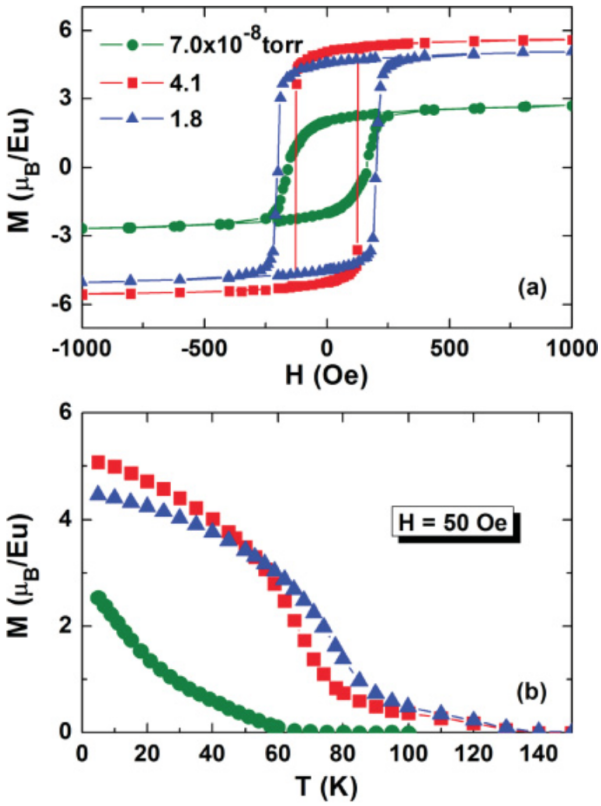

Figure 3-5 The magnetic properties of EuO films deposited under different oxygen pressures. The upper panel shows hysteresis loops measured at 4.5K. The lower panel shows the magnetizations vs. temperature.

Tunnel junctions with MgO/EuO hybrid barriers were then fabricated. The first MgO barrier deposited on bcc-Fe is epitaxial (100). MgO not only function as a symmetry filter to enhance the coherence, but also act as a spacer layer to avoid the direct exchange coupling between the electrodes (Fe) and spin filter layer (EuO). The lattice constant of EuO is 5.142 Å while that of MgO is 4.211 Å. It is possible to use specific growth conditions to create epitaxial growth. However, in that work, EuO was deposited at room temperature, therefore the barrier lost epitaxy after the MgO layer. As shown in Figure 3-6, XRD (X-Ray Diffraction) clearly revealed that EuO was polycrystalline. The TMR behavior is shown in Figure 3-7, the maximum TMR reached was 40% at 1K.

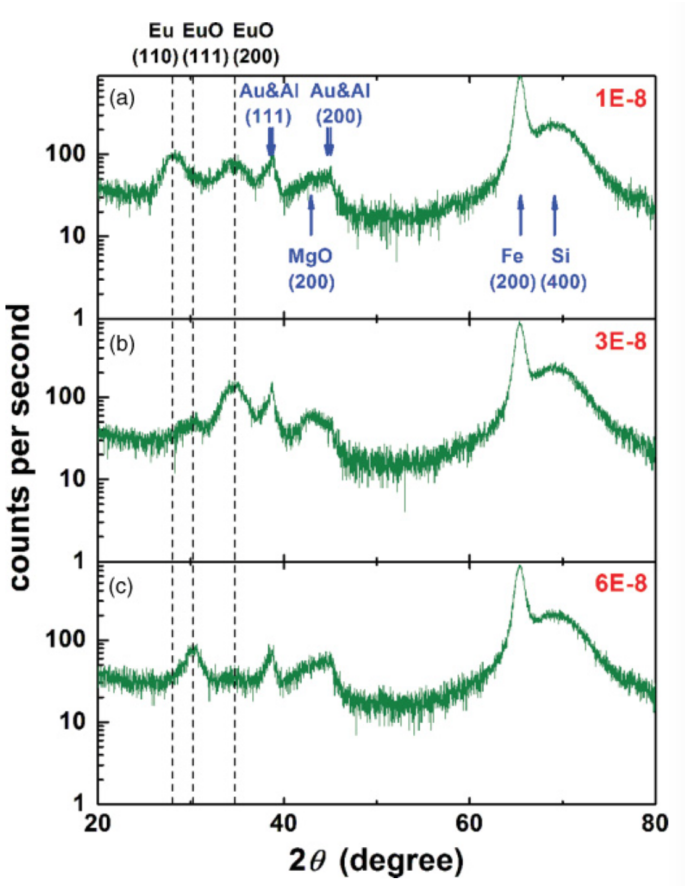

Figure 3-6 XRD of Si/ 5nm MgO/ 20nm Fe/ 2nm MgO/ 3nm EuO/ 3nm Y/ 50nm Al/ 30nm Cr/ 5nm Au junctions. It lost epitaxy after the 2nm MgO barrier layer therefore the EuO is polycrystalline.

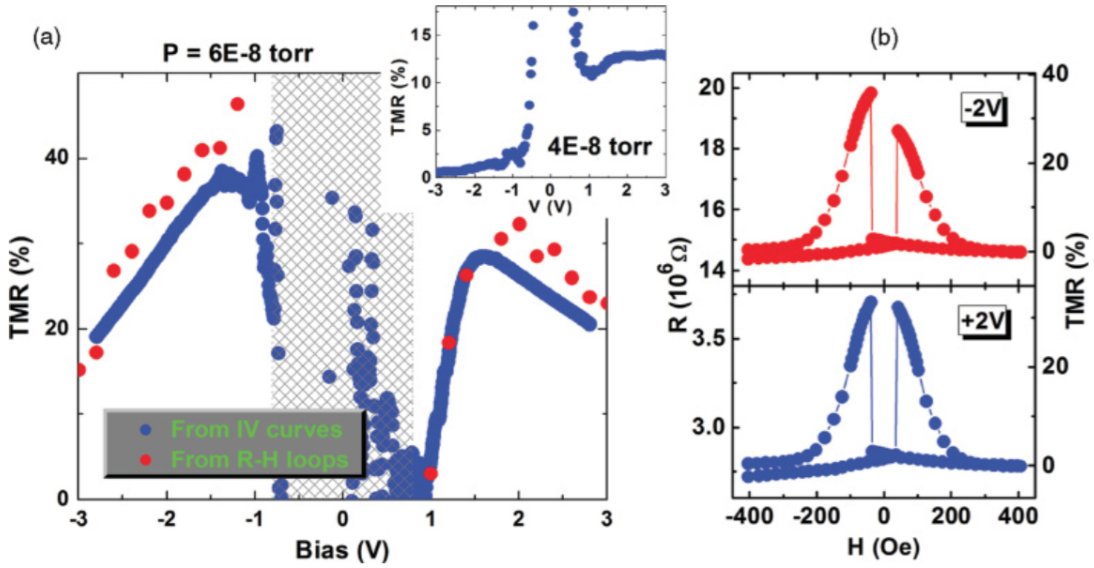

Figure 3-7 TMR of the above mentioned junction, with the EuO grown at the oxygen pressure of 6×10^{-8} torr. The left panel shows the TMR bias voltage dependence. The Blue points were deduced from IV curves, while the red points from Resistance-Magnetic fields measurements. A comparison graph, with EuO grown at the oxygen pressure of 4×10^{-8} torr, is shown in the middle upper insert. The right panel shows some actual Resistance-Magnetic fields diagrams.

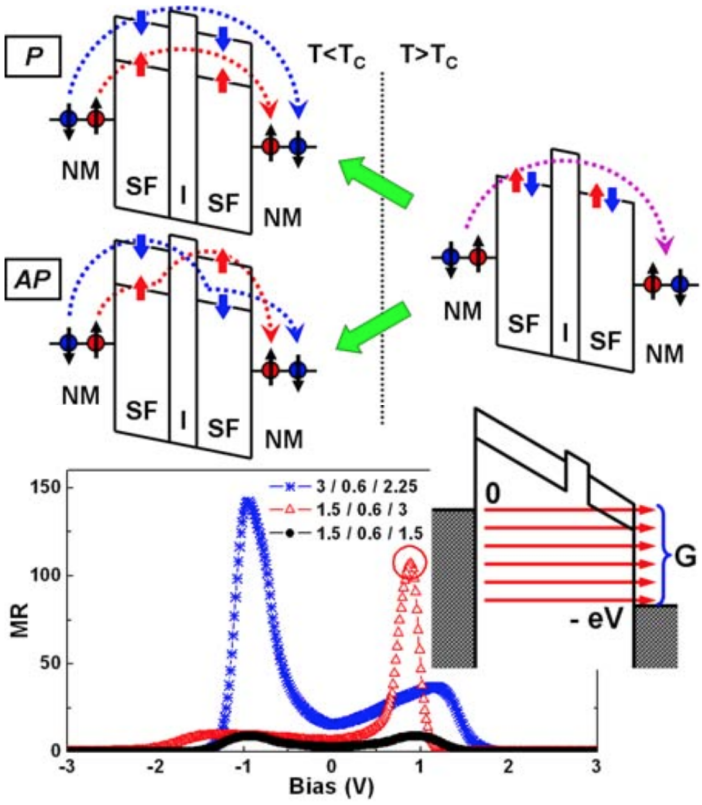

Figure 3-8 The operation principle of the double spin filter tunnel junctions. The dotted lines in the upper diagram show the barrier heights that the spin up (red) and down (blue) electrons have to cross over. The lower diagram shows the calculated TMR bias dependence [68].

The MIT group also used two EuS layers to build double spin filter junctions with Al electrodes. The operation principles of double spin filter mechanism is shown in Figure 3-8, and Figure 3-9 shows the MR loops and the bias dependence of an example double spin filter tunnel junction. The dotted lines in the upper diagram show the path that the spin-up and -down electrons have to cross over. Clearly, in the antiparallel configuration, both channels face a tall barrier which leads to a higher resistance state. The lower diagram shows the calculation of MR bias dependence. Three different labels indicate three kinds of junctions with the thicknesses labelled in nanometers for the composite barrier: EuS/Al2O3/EuS. The insert shows that the total conductance is the integration of the tunnel probabilities of every possible state under a fixed external bias. The red circle marks the

peak of the MR, and it corresponds to the Fermi level of the left electrode aligned above the tunnel barrier edge on the right side, namely, enhanced by the Fowler-Nordheim tunneling [68,69].

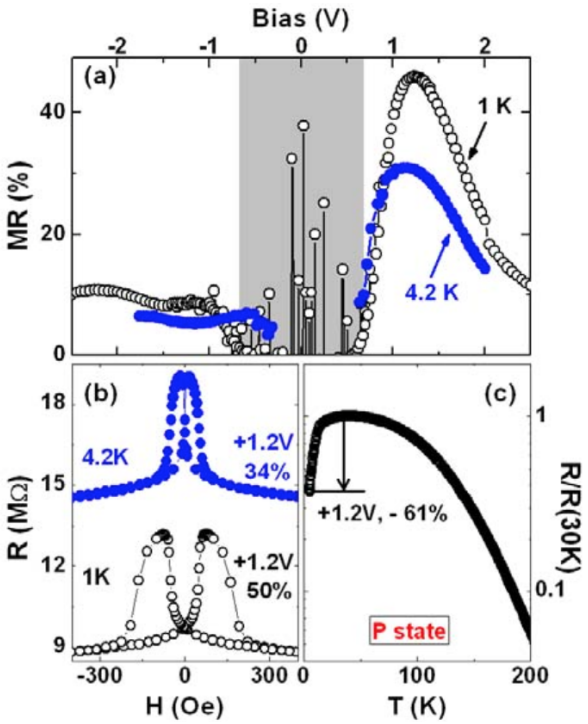

Figure 3-9 The magnetic resistance of a double spin filter tunnel junction with 10nm Al/ 1.5nm EuS/ 0.6 Al2O3/ 3nm EuS/ 10nm Al. (a) is the bias dependence at 4.2K and 1K. Because of the huge impedance, the low bias part (shaded region) before the onset of Fowler-Nordheim tunneling is too noisy to measure. A few example MR loops are shown in (b). (c) shows the resistance of the junction as a function of temperature, measured under 1.2V bias [68]. The resistance drop indicates a reduction on the (spin-up) tunnel barrier height.

In general, the papers above discussed the magnetic properties of several spin filters and how we can make MgO and ferromagnetic spin filters work together. Firstly, MgO acts as a symmetry filter to improve the spin and wave function coherence. Secondly, MgO breaks the magnetic coupling between the bottom electrode and the spin filter such that we can generate the antiparallel configuration. Thirdly, EuS is one of the most studied spin filter material due to the large splitting of conduction band. Furthermore, it is well lattice-matched with MgO (with only 0.2% mismatch) and should therefore grow epitaxially on MgO. In this thesis, we decided to use epitaxial MgO to couple

with epitaxial spin filter EuS, as a demonstration of principle, to create the type of symmetry & spin filtering hybrid tunnel junctions.

Chapter 4
Experimental

This chapter gives the readers detailed steps to grow the epitaxial FeCo/MgO/EuS magnetic tunnel junctions mentioned above. The system used is ATC ORION dual chamber deposition system from AJA International.

4.1 Electron Beam Physical Vapor Deposition

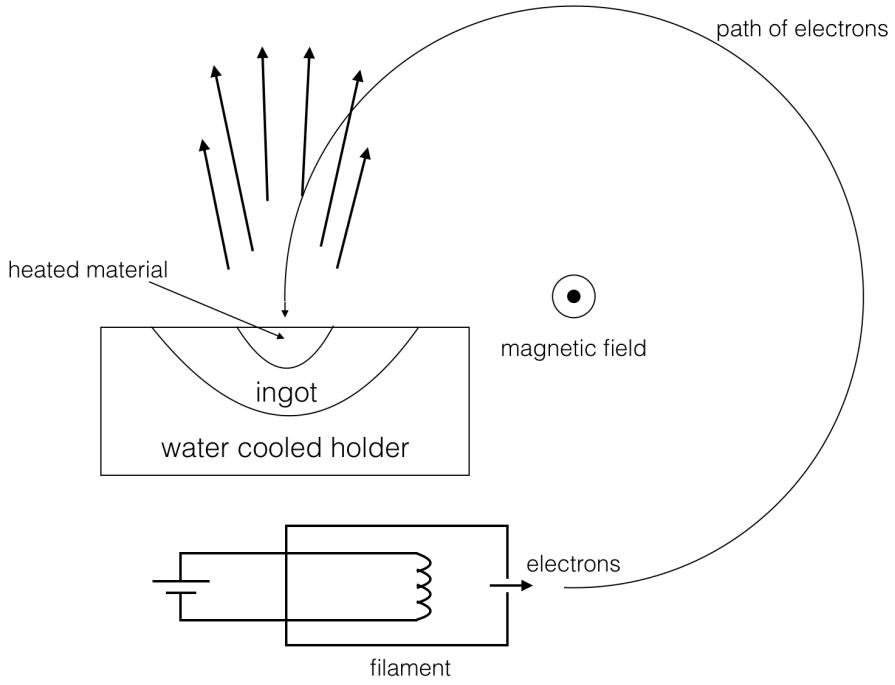

Figure 4-1 The basic structure of the high vacuum electron-beam evaporation system

The FeCo/MgO/EuS junction is fabricated with the high vacuum electron beam evaporation system illustrated above. As you can see in Figure 4-1, there is a filament at the very bottom which is made of tungsten. The filament is heated with high current to generate thermal electrons, and these electrons are extracted by a high voltage to generate an electron beam. Under the effect of the

magnetic field within the system, the electron beam is bent by 270° and hit the source material. The electrons will deposit all their kinetic energy and generate a very high temperature on the source. After the source material reaches the evaporation temperature, it will be vaporized and deposited onto the Si substrates positioned facing the source.

In this thesis, we also used a set of shadow masks to build the patterns of the tunnel junction devices. We load all the shadow masks, including the ones for bottom and top electrodes and the junction definitions, into the loadlock together with the substrate, so that we can exchange the masks in situ and make sure our whole processes are completed under high vacuum condition. Detailed growing procedures and preparation are discussed in 4-2. Figure 4-2 is the basic operation principle of the shadow masks. All the holders, masks are cleaned by heating at 300°C on a regular basis.

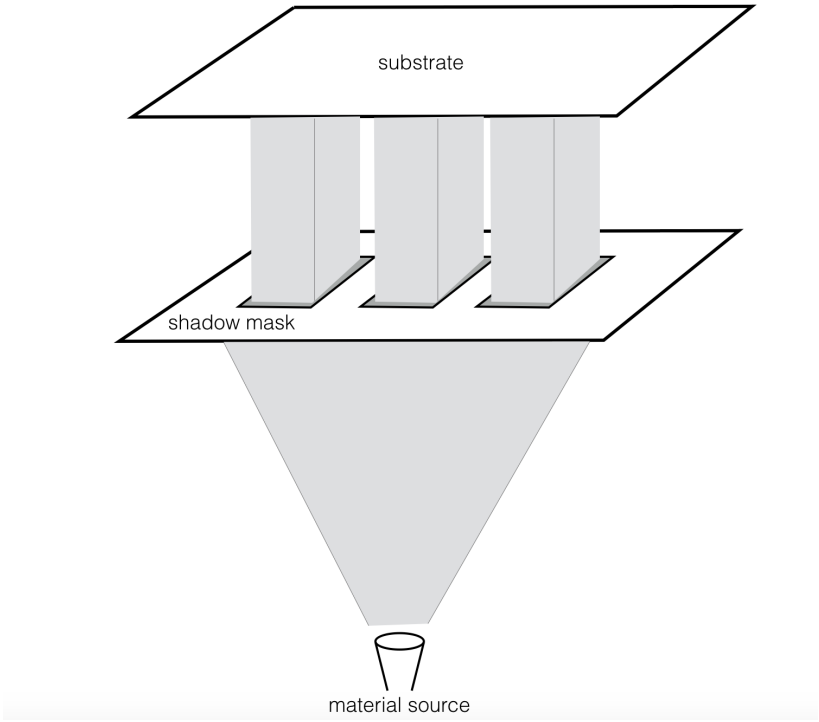

Figure 4-2 The basic principle of shadow masked evaporation. For the mask regions that are hollow, source materials can travel through and deposit onto the substrate, therefore transferring the shadow mask patterns onto the substrate.

4.2 Preparation of Magnetic Tunnel Junctions

The Magnetic Tunnel Junction is grown on a HF cleaned Si (100) wafer, which is first buffered with 10 nm epitaxial MgO deposited at 300°C. The tunnel barrier of the junction is epitaxial MgO/EuS, which is sandwiched by ferromagnetic FeCo, as the bottom electrode, and nonmagnetic Ti, as the top electrode. The deposition of our samples is through an electron beams (e-beam) system. The high vacuum e-beam system has a decent pressure better than 1×10^{-8} Torr during the whole growth process. According to the AFM (atomic force microscope) measurement results, we choose 0.08 Å/s to be the growth rate of each layer to ensure small roughness and good interface quality in our junctions. Due to the humidity sensitivity of the junctions (especially MgO), our samples are in situ patterned with shadow masks rather than using wet lithography. Furthermore, the samples are sealed in dry N2 till the transport measurement.

Step 1: Cleaning of the Wafer

Due to the natural oxidization of the Si wafer, there will be a thin layer of SiO2 on the wafer. Hence, every time we fabricate our samples, we need to clean the wafer beforehand. The solution is that we etch the silicon wafer with 1% buffered HF after doing solvent ultrasonic cleaning in IPA.

Figure 4-3 Clean the wafer with 1% HF after doing ultrasonic cleaning by dipping into IPA.

Step 2: Deposition of the Buffer Layer

After loading the wafer into the chamber, we heat the sample holder to 300°C before depositing 10nm MgO as the buffer layer. This MgO layer is (100) epitaxial with Si (100).

Figure 4-4 Deposit 10nm MgO (100) as the Buffer layer after heating the holder for 1 hour under 300°C

Step 3: Deposition of the bottom electrode

We deposit 5.5nm FeCo after the holder cooling down for 2 hours from 300°C (approximately reaching 100°C) to keep the bottom electrode epitaxial. The reason why we choose 5.5nm as the FeCo thickness is that if we decrease the FeCo thickness, we will more likely get discontinued bottom electrodes. If we increase its thickness, the coercive fields of FeCo and EuS will be too close to be distinguished, making it difficult to create the antiparallel state.

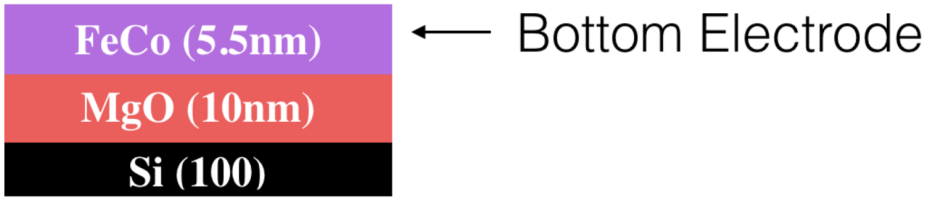

Figure 4-5 Deposit 5.5nm FeCo (100) through the bottom electrode shadow mask after cooling down the system from 300°C for 2 hours (approximately reaching 100°C)

Step 4: Deposition of the MgO tunnel barrier

Right after the deposition of the bottom electrode, we then grow the first tunnel barrier of MgO; we tried several thicknesses of MgO to verify whether the tunnel barrier thickness will affect the TMR of the junctions, detailed results are discussed in chapter 5.

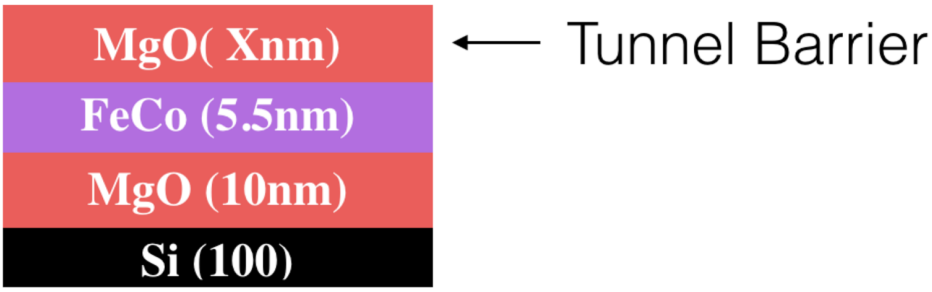

Figure 4-6 Deposit MgO (100) as the first part of the tunnel barrier, several thicknesses were attempted.

Step 5: Deposition of the EuS spin filter

Optimized from our experiences, we grow the EuS layer by further cooling down the system two more hours after the deposition of the MgO tunnel barrier (approximately reaching room temperature), such that we could have a better temperature-tuned hysteresis loop from EuS. The EuS coercive field increases as the deposition temperature increases [68]. Here we choose 3nm to be the thickness of the spin filter because it gives us the best TMR among the few attempted thicknesses, 1nm, 2nm and 4nm. We will discuss this also in the next chapter.

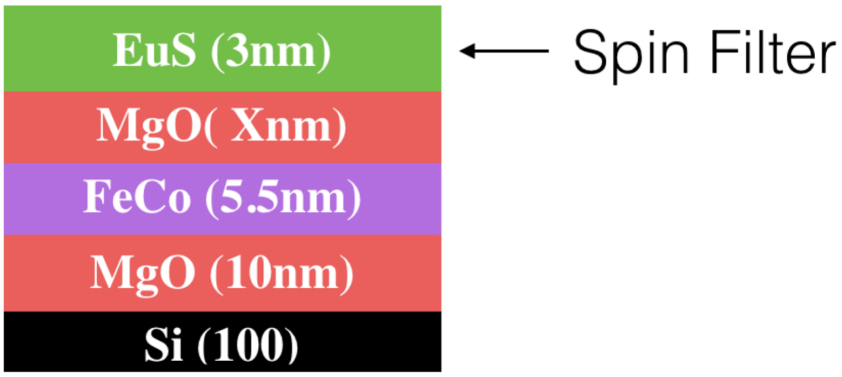

Figure 4-7 Deposit 3nm EuS onto the tunnel junction layer after 2 hours cooling, it is (100) epitaxial.

Step 6: Deposition of the junction Definition layers

From the previous experiences, we choose to use definition layers to shrink the active junction area, in order to avoid having pinholes by decreasing the active junction size. In this experiment, the final active area of the junction is 30μm ×30μm.

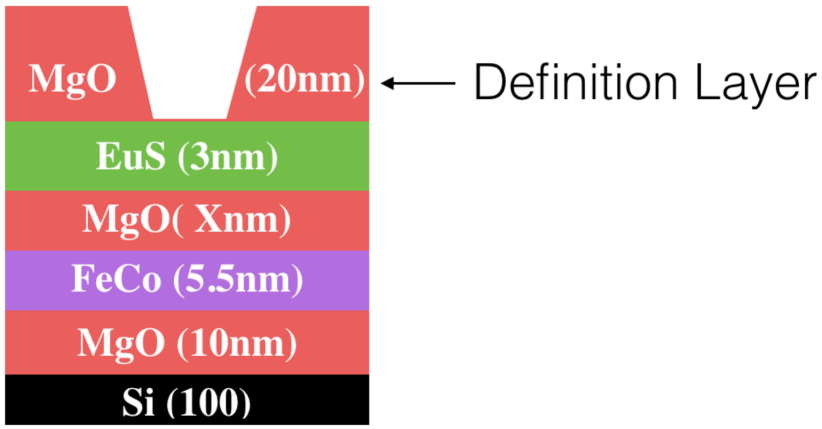

Figure 4-8 Deposit 10nm + 10nm MgO definition layer onto the EuS. The definition layer is polycrystalline and insulating, only to define a smaller active junction area.

Step 7: Deposition of the top electrode

To finish the junction up, we deposit 10nm Ti as our top electrode using the top electrode shadow mask.

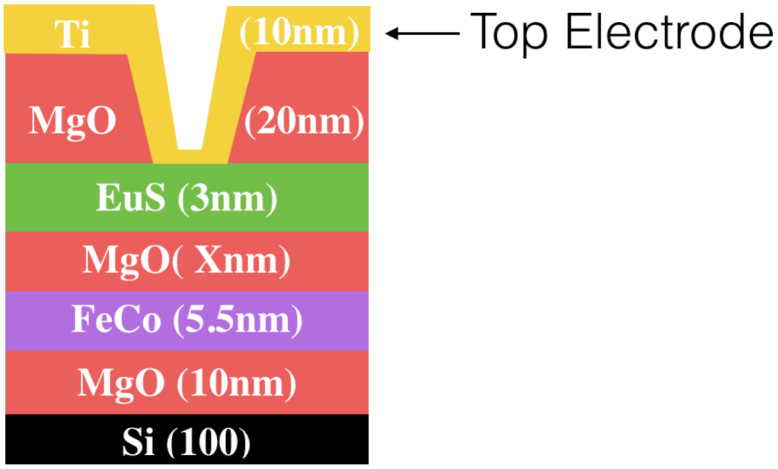

Figure 4-9 Deposit 10nm Ti as the top electrode, it is polycrystalline

Step 8: Protection

After finishing fabrication of the whole junction, we either immediately seal it into dry N2 bags, or deposit 3nm TiN plus 3nm Al2O3 as a protection layer after Ti.

4.3 Measurement of Magnetic Tunnel Junctions

The structural properties of the junctions are characterized using XRD (X-ray diffraction, on BRUKER D8 ADVANCE), which measures each layer's crystal structure to verify the epitaxy of the junction.

The transport properties of the samples are measured using two-terminal method as Figure 4-10 shows. Because of the relatively high impedance of the double barrier junctions, two-terminal measurement does not induce much error to the results. All the samples are measured in sweeping magnetic field in the range of -300G and 300G. We used liquid helium to make sure our standard measurements are all at 4K, and we also used heater to adjust the sample temperature from 4K to 21K with the deviation no more than 0.05K.

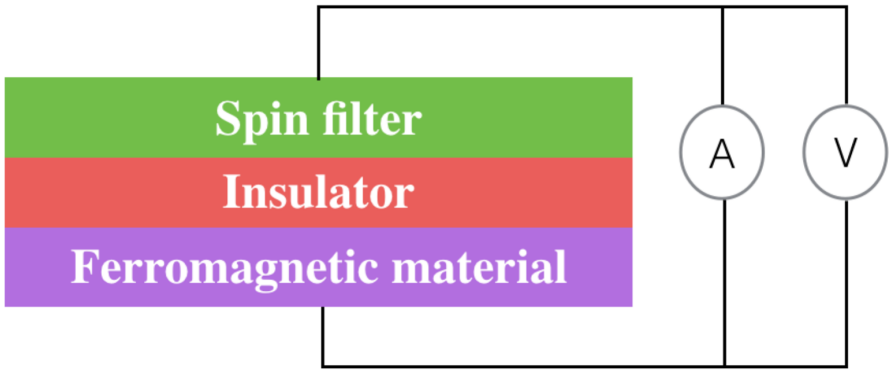

Figure 4-10 The electrical transport properties of the samples are measured with two-terminal method

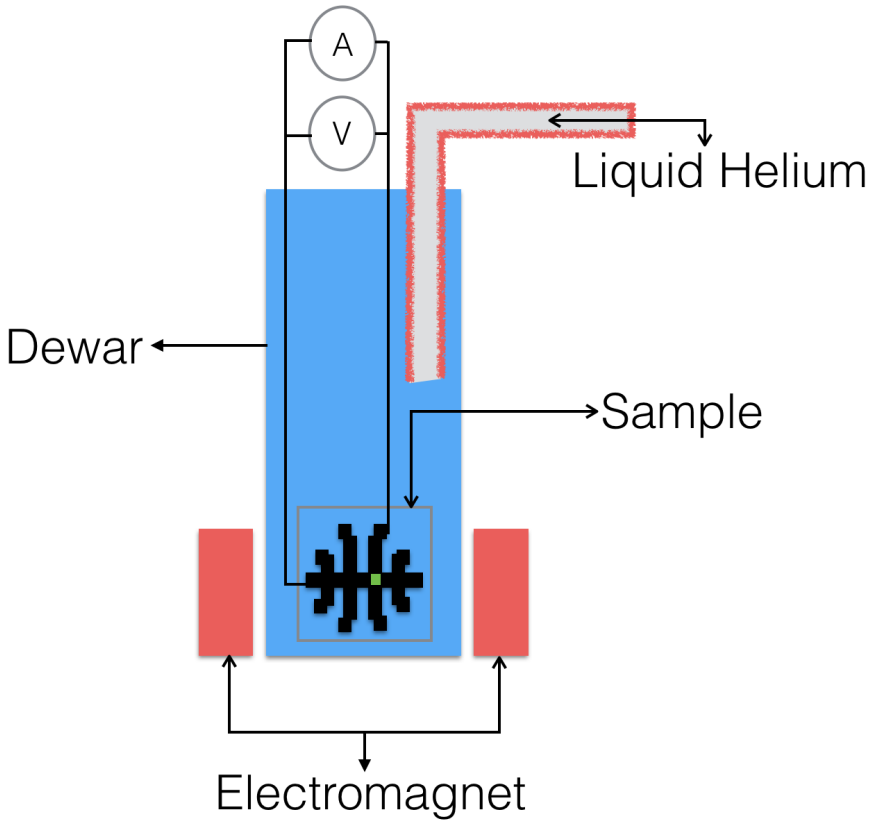

Figure 4-11 Schematic diagram of the low temperature transport measurement setup

Chapter 5
Results and Discussions

This chapter provides the experimental results, detailed analysis, and further discussions based on the outcomes.

5.1 Epitaxial Growth of FeCo/MgO/EuS(100)

XRD confirmed the epitaxy of the sample stack. According to our previous experience, MgO is epitaxial on Si (100) when deposited at 300°C [10].

In this experiment, we used FeCo as the bottom electrode instead of Fe, because it leads to higher spin polarization when coupled with MgO [70]. But when we tried to deposit FeCo onto the MgO buffer layer at room temperature, after checking with XRD, we found FeCo (110) peaks indicating that the layer was polycrystalline. We then tried to grow FeCo at several higher temperature and found that the best condition so far is at 2 hours cooling down after the MgO deposition (approximately 100°C), and we found only the FeCo (200) peak at 65.262 degrees, as you

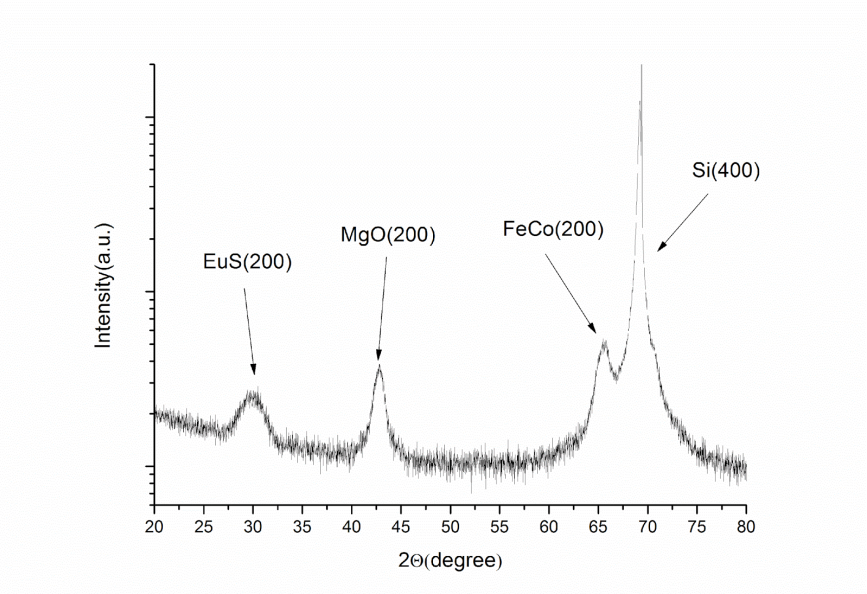

Figure 5-1 High-resolution θ-2θ scans of the magnetic tunnel junction: Si (100)/10nm MgO/ 5.5nm FeCo/3nm EuS.

can see in Figure 5-1.

Theoretically, the bulk lattice parameters of MgO and FeCo are 4.212Å and 2.857Å, with approximately a $\sqrt{2}$ relation, which means FeCo layers are 45° rotated in plane relative to both MgO (100) and the Si substrate in order to form the best lattice matching. We then tried to grow EuS at several temperatures by cooling another 1h, 2h, 3h, and 4h after depositing the MgO buffer, all of which showed the spin filter layers perfectly epitaxial, and the EuS (200) θ-2θ peak at the expected 29.929 degrees.

We also performed off-axis ψ scan on the FeCo (110) and EuS (220) reflections to verify that they are indeed epitaxial instead of textured. Because the (100) orientation is off the z-axis by 45°, if we tilt the sample by 45° then rotate it around the z axis (Ψ scan) by 360°, we will detect the {110} class of peaks four times. The stronger and narrower the peaks, the better quality of the epitaxy. As you can see from Figure 5-2, the four sharp peaks are from Si {220}, and the four relatively wider peaks are from FeCo {110}. Si peaks show up because they are so strong coming from the single crystal wafer, even though we are targeting the FeCo {110}. In Figure 5-3, the sharp peaks are still from Si (220), and the ones directly under the Si peaks are from EuS {220}. So we can determine that FeCo are indeed 45° rotated in plane relative to both EuS and Si. In Figure 5-2 and 5-3, we could see both FeCo and EuS peaks, 45° apart, because their diffractions are close to each other.

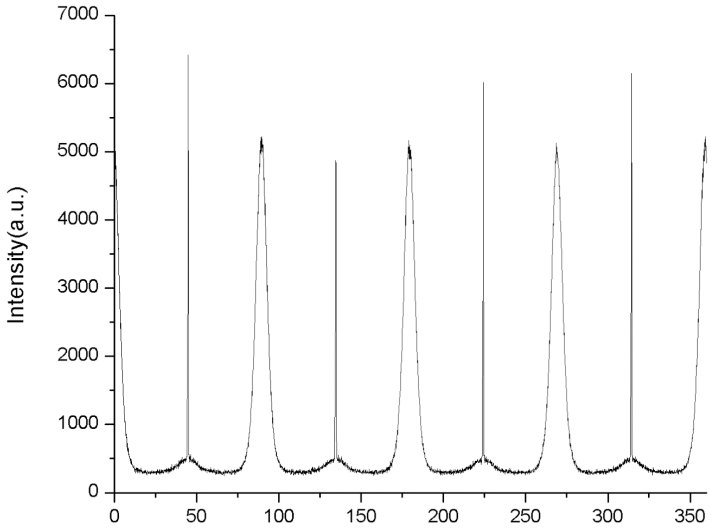

Figure 5-2 Off-axis ψ scan on the FeCo (110) reflections. Si (100)/ 10nm MgO/10nm FeCo/2nm MgO/3nm EuS/ 5Ti

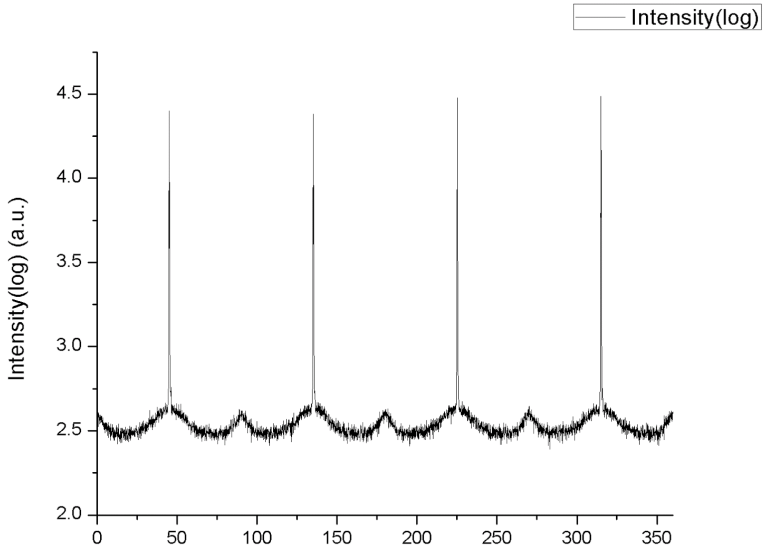

Figure 5-3 Off-axis ψ scan on the EuS (220) reflections. Si (100)/ 10nm MgO/10nm FeCo/2nm MgO/3nm EuS/ 5Ti

5.2 The Effect of EuS as a Spin Filter

The spin filtering can lead to the difference of the tunneling probabilities of spin up and spin down electrons, which therefore has similar effects as ferromagnetic materials in generating spin currents. In our experiment, we tried to measure the TMR under several temperatures above and below Tc (16.5K) of EuS to see whether the spin filter behaves as a substitution of ferromagnetic materials. When the temperature is under 16.5K, we found that EuS gives us a large TMR effect, as you can see in Figure 5-4 and 5-5, the TMR reached 25% at 5K, but decreased to no more than 2.5% at the temperature of 19K, and no TMR was measured when the temperature is greater than 21K.

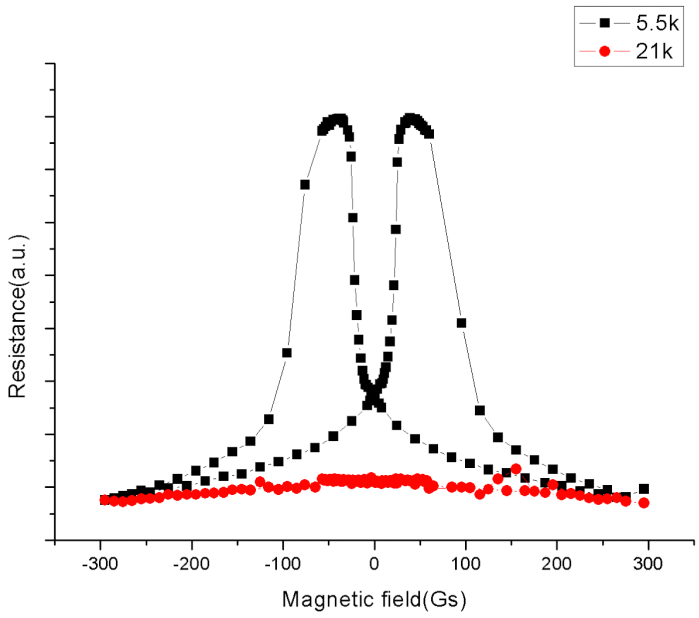

Figure 5-4 TMR of the junction 5.5nm FeCo/1nm MgO/3nm EuS at 5.5K and 21K.

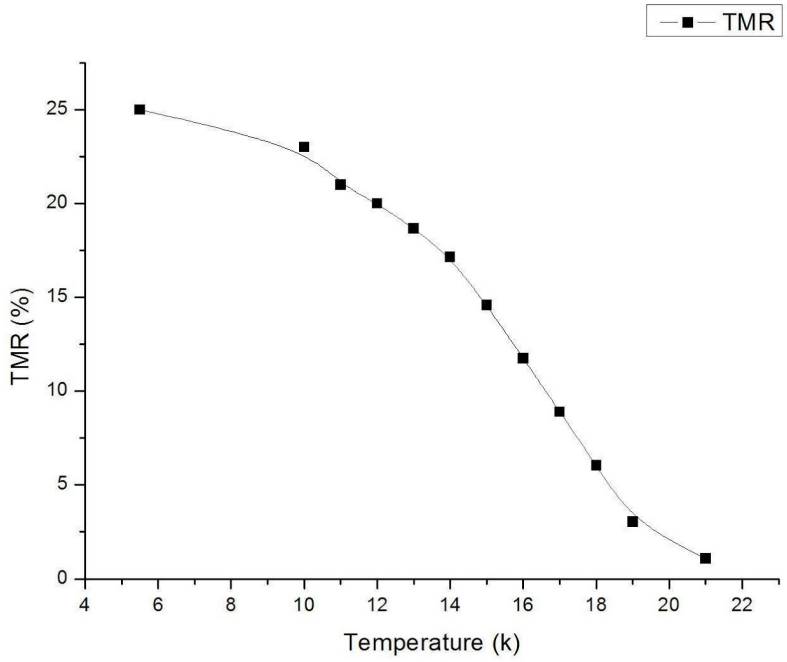

Figure 5-5 TMR ratio of the junction 5.5nm FeCo/1nm MgO/3nm EuS/ 10nm Ti between 5.5K and 21K, the applied current is at 10 nA.

5.3 The Elemental Characteristics of FeCo/MgO/EuS

The junctions have also been analyzed by X-ray Photoelectron Spectroscopy (XPS). The depth profile is shown in Figure 5-6. Depth profile is a technique that measures the concentration (y-axis) in relation to depth (x-axis). In the XPS system, the composition over depth was obtained by repeated sputter removal of the surface materials. After first sputtering 500s to get through the protection layer Al2O3, the 3nm TiN and 10nm Ti shows up. We can clearly see Mg starts right after EuS, and the spread of Mg is likely because the light Mg atoms have been knocked into FeCo in the sputter process. The chemical distribution of elements clearly matches our desired structure, with some complications showing up at the interfaces due to the intermixing.

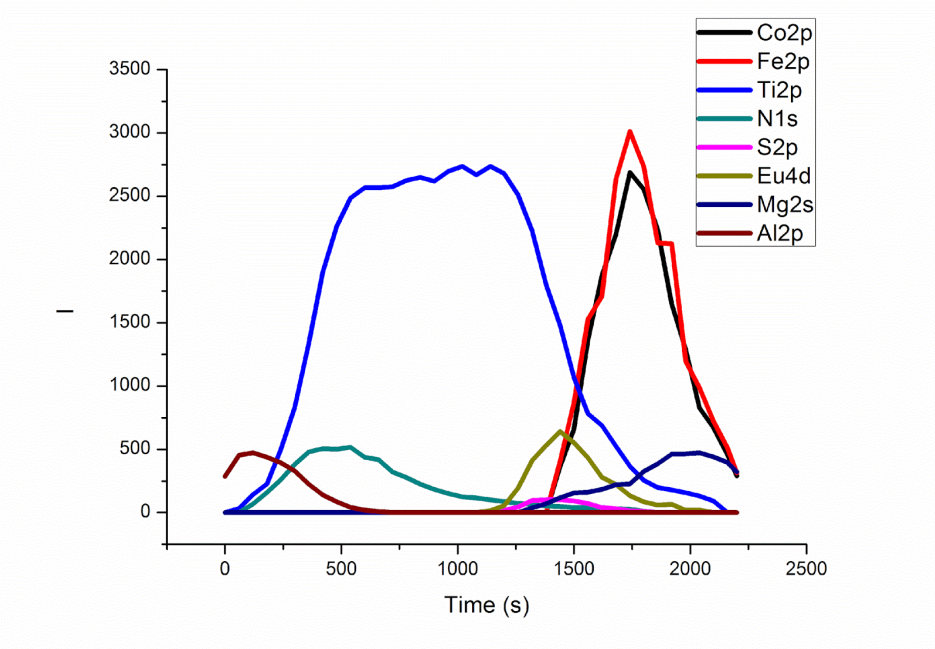

Figure 5-6 XPS depth profile of the junction Si (100)/10nm MgO/5.5nm FeCo/1.5nm MgO/3nm EuS/10nm Ti/3nm TiN/3nm Al2O3

5.4 TMR of Tunnel Junctions with different MgO Thickness

In this thesis work, the best TMR we have obtained is with the MgO tunnel barrier at 1nm and EuS at 3nm. In terms of the spin filter layer thickness, we tried 1nm, 2nm, 3nm, and 4nm EuS and found that 3nm EuS gives us the best TMR. If we further increase the thickness of EuS, the resistance of the junctions will become too large to yield reasonable TMR. On the thick end, multistep hopping dominates and more spin-flip scatterings occur [44,71,72]. Reversely, if the thickness of EuS is too thin, the EuS layer will not have sufficient spin filtering capability which goes up with thickness [11]. Hence, we decided to use 3nm EuS for all other comparison groups, making sure the single variable we have is the MgO thickness. In the best junctions, the resistance of the 1nm MgO / 3nm EuS junction is around 30kΩ at room temperature. At first, we tried 0.5nm, 1 nm, 1.5nm and 2nm for MgO, which, as we expected, have the resistance over the range between 10kΩ and 5MΩ. The TMR ratio reached 4.2% in 0.5nm MgO samples, 64% in 1nm ones, and it dropped back to 2.9% when the tunnel barrier is 1.5nm, and no TMR has been found when MgO is 2nm. After that,

we further tried 0.8nm and 1.2 nm MgO to see whether there truly is a maximum TMR at around 1nm, and we also tried growing junctions even without MgO in the tunnel barrier. We got 13% and 17.8% at 0.8nm and at 1.2nm MgO respectively, we did not get any TMR when there is no MgO tunnel barrier, which can be attribute to the interlayer magnetic coupling [21]. Figure 5-7 shows the magnetoresistance vs bias voltage for these junctions. The TMRs are mostly symmetric in voltage bias. 1nm MgO(blue) MTJs have the largest TMR as high as 64%. The TMR of 0.8nm MgO(red) and 1.2nm MgO(green) junctions drop to 13% and 17.8%. For the ones with 0.5nm and 1.5nm MgO, the TMRs are less than 5% and are negligible compared to the 1nm MgO junctions.

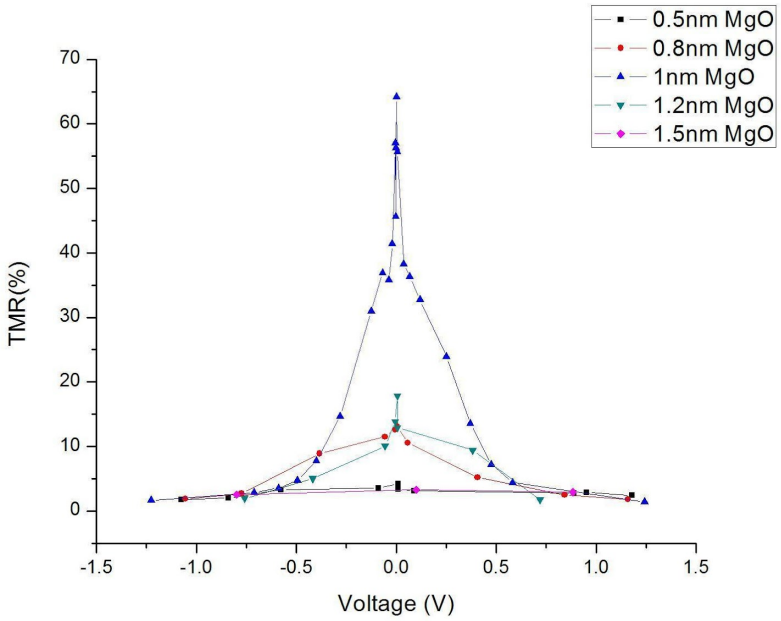

Figure 5-7 TMR of difference Thickness of MgO (0.5nm, 0.8nm, 1 nm, 1.2nm, 1.5nm)

These junctions have standard I-V curves, which are non-linear indicating tunneling behavior [46], as seen in Figure 5-8. The dramatic increase of tunnel current above 1V is due to the appearance of Fowler-Nordheim tunneling, happening when the applied bias is higher than the potential barrier. Figure 5-9 shows the TMR at different tunnel barrier thickness and we can see a maximum TMR at 1 nm MgO.

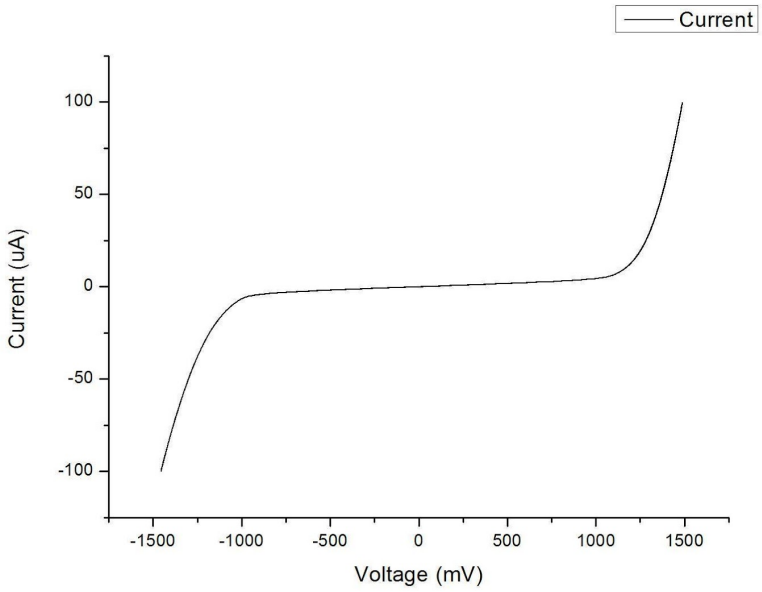

Figure 5-8 I-V characteristic of the junction of 0.5nm MgO as tunnel barrier

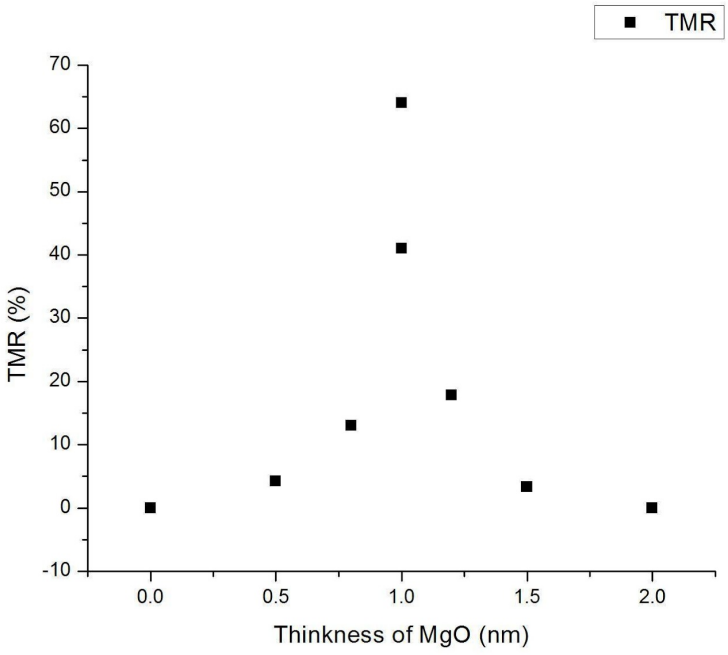

Figure 5-9 TMR at different MgO tunnel barrier thickness. The EuS thickness is kept at 3nm. The 1nm MgO samples were attempted twice, both revealed significantly larger TMR than other

thicknesses. Small uncertainty in the thickness control prevents the samples to be exactly the same, due to the sensitivity of the TMR near this thickness.

Because of the similarity of the crystal structures of EuS and MgO, the electrons should maintain their Bloch wave symmetry and will not have much spin scattering in the tunnel barrier, which should increase the spin transport efficiency. There are four Bloch states relevant to the transport, among which, the $\Delta 1$ states have the slowest decay rate. As MgO grows thicker, $\Delta 1$ states will be the main contributor and only fully spin-polarized electrons (from FeCo) can tunnel through the barrier, which will also enhance the spin transport efficiency. However, if we continue to increase the thickness of MgO, we found the TMR of the junctions decreased quite significantly, which demonstrates that there are some differences in the band structures between these two materials. The band structure of EuS has been shown on Figure 5-10 [29]. Compared to the MgO band structure, we can clearly see that the Γ point is no longer the conduction band minimum. Even though the symmetry is still permitting the $\Delta 1$ states to tunnel through easily, additional tunneling is permitted at the X point. More complications arise because the valence band maximum is now formed with 4f bands, which does not match any of the bands coming from FeCo/MgO. The $\Delta 1$ symmetry tunneling prefers to travel near the Γ point, while the EuS spin filtering prefers electrons going along the X point. As a result, although we did get some fairly good tunneling coherence, it vanishes faster than we had anticipated.

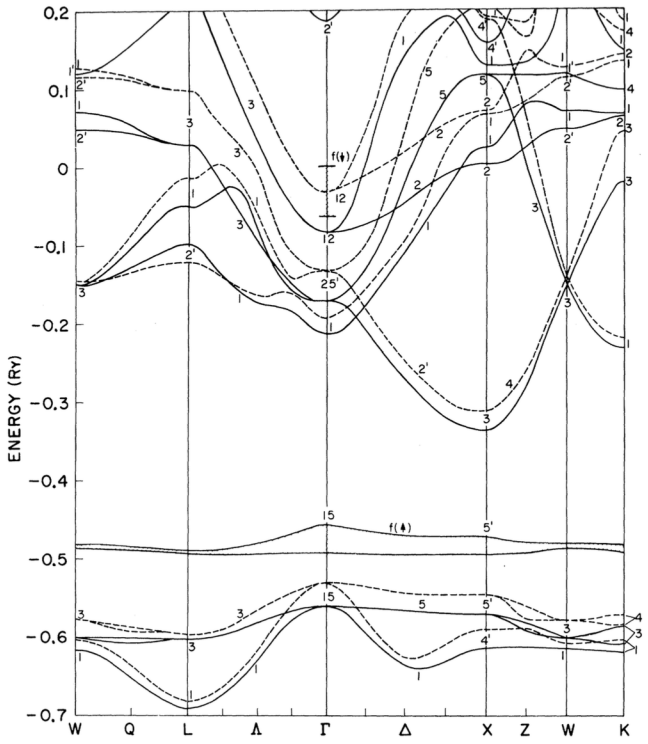

Figure 5-10 Energy bands of EuS. Spin-up electrons are depicted by solid lines, spin-down electrons are depicted by dash lines. The lowest point on the conduction bands - point 3, is what determines the tunnel barrier heights of the EuS layer.

Chapter 6
Future Work

We have also tried with Fe as the bottom electrode of the junction, but the junction resistance was always too small, so that we could not measure the transport properties of the junctions. In principle, there should be no problem to replace FeCo with Fe. When we do the AFM on the junctions with Fe electrodes, it turned out that the roughness is very large (around 3nm) when tunnel barrier MgO was grown on Fe. To the best of our knowledge, the junctions shorting may be due to the pinhole formation; so, we can try the Fe electrodes-based spin filter tunnel junction after solving the pinhole problems, for example, with micro/nana-fabricated junctions. In addition, annealing in UHV is known to reconstruct the Fe surface and makes it much smoother [68], therefore we could try to improve our devices by using UHV deposition systems, such as in MBEs, and test suitable growth and annealing temperatures.

The growth condition plays a key role in increasing the TMR. Because the interface between two layers and the periodical location of the atoms are determining the coherence and transport efficiency in the transportation properties. Even very small difference of growth conditions will affect the transportation results of the junctions. For now, we are using 0.08Å/s growth rate for all the layers, we could use AFM to detect each layer's roughness and try to find the best growth rate for every layer, in order to reduce the roughness of the interfaces and increase the quality of the layers. Further moving to UHV systems will dramatically improve the interface quality as well. In an UHV environment, we can also take the time to fine tune the growth temperature of each layer without worrying about surface degradation. Optimized growth temperatures can enhance the crystal quality therefore the tunneling coherence.

We have also tried to use Mg insertion method as mentioned before. The reason we want to use Mg insertion is because we will deposit MgO after the growth of FeCo layer, which will generate O partial pressure into the chamber. FeCo has the tendency to be oxidized, like Fe did [26]. After doing Mg insertion before the deposition of MgO, Mg will instead absorb oxygen and become MgO. So we can consider Mg insertion to have the same effect as a MgO deposition, except that it to a large extent prevents oxidation on the bottom electrode. However, when we use Mg insertion in our junctions, the TMR results are not as good as the ones without using Mg insertion. We tried it a few

times on several thicknesses of MgO, all the results showed that the junctions' TMR decreased. In the experiment, we found that oxidization of bottom electrodes are not significant so we did not apply Mg insertion further, but Mg insertion is something worth further exploring and in principle it should help further improving the devices.

In the near future, we could also try to use the post annealing process. Post annealing has been widely used in the junctions with MgO tunnel barriers. This technique is now industry standard for enhancing the performance of MgO MTJs, especially the sputter deposited ones. When using Fe as our electrodes, we encountered the problems of high roughness and pinhole formation. In that case, we could potentially use post annealing to improve the quality. In doing post annealing, atoms migrate in the crystal lattice and the number of structural defects can be decreased, which can reduce the roughness, avoid pinholes, and increase the quality of the devices.

Flash annealing is another way to improve the magnetic properties of the MTJs. In doing this, MTJs are rapidly heated then followed by rapid cooling, with the whole process happening in seconds. The rapid heating during flash annealing can assist the kinetics of crystallization [36], which improves the quality of the crystallization products; at the same time, the fast process prevents undesired diffusion between materials, notably Mn diffusion towards the barrier when antiferromagnetic pinning is present.

So far, the MTJs we used can only operate at low temperature due to the low Curie temperature of EuS. The system was chosen as a demonstration of principle, and through thickness variations, we encountered a band matching/competition issue that had not been reported before. However, coherence and spin polarization at room temperature is the ultimate goal of the spin-based information processing. There are some other ferromagnetic insulating materials, such as many ferrites and perovskites, with their Curie temperature well above room temperature. NiFe2O4 and CoFe2O4, as the insulating relatives of Fe3O4, have exchange splitting on the conduction band of 0.8eV and 1.2eV [28], therefore have the potential to function as room temperature spin filters.

References

[1] Åkerman, Johan. "Toward a universal memory." Science 308.5721 (2005): 508-510.

[2] "Past, Present and Future of MRAM", NIST Magnetic Technology, 22 July 2003

[3] Kate McAlpine, "Spin flip trick points to fastest RAM yet",NewScientist, 13 August 2008

[4] Ousterhout, John, et al. "The case for RAMClouds: scalable high-performance storage entirely in DRAM." ACM SIGOPS Operating Systems Review 43.4 (2010): 92-105.

[5] M. Julliere (1975). "Tunneling between ferromagnetic films". Phys. Lett. 54A: 225–226.Bibcode:1975PhLA...54..225J. doi:10.1016/0375-9601(75)90174-7.

[6] T. Miyazaki and N. Tezuka (1995). "Giant magnetic tunneling effect in Fe/Al2O3/Fe junction". J. Magn. Magn. Mater. 139: L231–L234. Bibcode:1995JMMM..139L.231M. doi:10.1016/0304-8853(95)90001-2.

[7] J. S. Moodera; et al. (1995). "Large Magnetoresistance at Room Temperature in Ferromagnetic Thin Film Tunnel Junctions". Phys. Rev. Lett. 74 (16): 3273–3276.Bibcode:1995PhRvL..74.3273M. doi:10.1103/PhysRevLett.74.3273. PMID 10058155.

[8] J. Mathon and A. Umerski (2001). "Theory of tunneling magnetoresistance of an epitaxial Fe/MgO/Fe (001) junction". Phys. Rev. B 63 (22): 220403. Bibcode:2001PhRvB..63v0403M.doi:10.1103/PhysRevB.63.220403.

[9] Butler, W. H., et al. "Spin-dependent tunneling conductance of Fe| MgO| Fe sandwiches." Physical Review B 63.5 (2001): 054416.

[10] Yuasa, Shinji, et al. "Giant room-temperature magnetoresistance in single-crystal Fe/MgO/Fe magnetic tunnel junctions." Nature materials 3.12 (2004): 868-871.

[11] Parkin, Stuart SP, et al. "Giant tunnelling magnetoresistance at room temperature with MgO (100) tunnel barriers." Nature materials 3.12 (2004): 862-867.

[12] S. Ikeda, J. Hayakawa, Y. Ashizawa, Y.M. Lee, K. Miura, H. Hasegawa, M. Tsunoda, F. Matsukura and H. Ohno (2008). "Tunnel magnetoresistance of 604% at 300 K by suppression of Ta diffusion in CoFeB/MgO/CoFeB pseudo-spin-valves annealed at high temperature". Appl. Phys. Lett.93 (8): 082508. Bibcode:2008ApPhL..93h2508I. doi:10.1063/1.2976435.

[13] Andrew R. Barron, Chemistry of the Main Group Elements. OpenStax CNX. Mar 22, 2014 http://cnx.org/contents/f46e8679-ee00-4073-9f5e-a87ca9955a9e@25.9.

[14] Roessler, D. M., W. C. Walker, and Eugene Loh. "Electronic spectrum of crystalline beryllium oxide." Journal of Physics and Chemistry of Solids 30.1 (1969): 157-167.

[15] N.O. Lipari and A.B. Kunz, Energy bands & optical properties of NaCl, Phys.Rev. B3, 491 (1971).

[16] Miao, G. X., et al. "Epitaxial growth of MgO and Fe/MgO/ Fe magnetic tunnel junctions on (100)-Si by molecular beam epitaxy." Applied Physics Letters 93.14 (2008): 142511.

[17] Miao, G. X., et al. "Disturbance of tunneling coherence by oxygen vacancy in epitaxial Fe/MgO/Fe magnetic tunnel junctions." Physical review letters 100.24 (2008): 246803.

[18] Meservey, Robert, and P. M. Tedrow. "Spin-polarized electron tunneling." Physics Reports 238.4 (1994): 173-243.

[19] Mavropoulos, Ph, N. Papanikolaou, and P. H. Dederichs. "Complex band structure and tunneling through ferromagnet/insulator/ferromagnet junctions." Physical review letters 85.5 (2000): 1088.

[20] Tsymbal, E. Yu, and D. G. Pettifor. "Modelling of spin-polarized electron tunnelling from 3d ferromagnets." Journal of Physics: Condensed Matter 9.30 (1997): L411.

[21] Miao, Guo-Xing, and Jagadeesh S. Moodera. "Controlling magnetic switching properties of EuS for constructing double spin filter magnetic tunnel junctions." Applied Physics Letters 94.18 (2009): 182504.

[22] Moodera, Jagadeesh S., and George Mathon. "Spin polarized tunneling in ferromagnetic junctions." Journal of magnetism and magnetic materials 200.1 (1999): 248-273.

[23] Miao G X, Münzenberg M, Moodera J S. Tunneling path toward spintronics. Reports on Progress in Physics, 2011, 74(3): 036501.

[24] Parkin S S P, Roche K P, Samant M G, et al. Exchange-biased magnetic tunnel junctions and application to nonvolatile magnetic random access memory. Journal of Applied Physics, 1999, 85(8): 5828-5833.

[25] Butler, William H. "Tunneling magnetoresistance from a symmetry filtering effect." Science and Technology of Advanced Materials 9.1 (2008): 014106.

[26] Ji, Yuan-Tao, et al. "Epitaxial growth of NaCl on Fe (100) and characterization of Fe/NaCl/Fe magnetic tunnel junctions." 14th IEEE International Conference on Nanotechnology. 2014.

[27] Matsumoto, Rie, et al. "Spin-dependent tunneling in epitaxial Fe/Cr/MgO/Fe magnetic tunnel junctions with an ultrathin Cr (001) spacer layer." Physical Review B 79.17 (2009): 174436.

[28] Holinsworth, B. S., et al. "Chemical tuning of the optical band gap in spinel ferrites: CoFe2O4 vs NiFe2O4." Applied Physics Letters 103.8 (2013): 082406.

[29] Cho, S. J. "Spin-polarized energy bands in Eu chalcogenides by the augmented-plane-wave method." Physical Review B 1.12 (1970): 4589.

[30] Tserkovnyak, Yaroslav, Arne Brataas, and Gerrit EW Bauer. "Spin pumping and magnetization dynamics in metallic multilayers." Physical Review B66.22 (2002): 224403.

[31] Greullet F, Tiusan C, Montaigne F, et al. Evidence of a symmetry-dependent metallic barrier in fully epitaxial MgO based magnetic tunnel junctions. Physical review letters, 2007, 99(18): 187202.

[32] Mather P G, Read J C, Buhrman R A. Disorder, defects, and band gaps in ultrathin (001) MgO tunnel barrier layers. Physical Review B, 2006, 73(20): 205412.

[33] Nozaki, T., N. Tezuka, and K. Inomata. "Quantum oscillation of the tunneling conductance in fully epitaxial double barrier magnetic tunnel junctions." Physical review letters 96.2 (2006): 027208.

[34] Lu, Zhong-Yi, X-G. Zhang, and Sokrates T. Pantelides. "Spin-dependent resonant tunneling through quantum-well states in magnetic metallic thin films." Physical review letters 94.20 (2005): 207210.

[35] Niizeki, Tomohiko, Nobuki Tezuka, and Koichiro Inomata. "Enhanced tunnel magnetoresistance due to spin dependent quantum well resonance in specific symmetry states of an ultrathin ferromagnetic electrode." Physical review letters 100.4 (2008): 047207.

[36] Jagielinski, T. "Flash annealing of amorphous alloys." Magnetics, IEEE Transactions on 19.5 (1983): 1925-1927.

[37] Djayaprawira D D, Tsunekawa K, Nagai M, et al. 230% room-temperature magnetoresistance in CoFeB/MgO/CoFeB magnetic tunnel junctions. Applied Physics Letters, 2005, 86(9): 092502.

[38] Miao, Guo-Xing, et al. "Inelastic tunneling spectroscopy of magnetic tunnel junctions based on CoFeB/MgO/CoFeB with Mg insertion layer." Journal of applied physics 99.8 (2006): 08T305.

[39] Moodera J S, Santos T S, Nagahama T. The phenomena of spin-filter tunnelling. Journal of Physics: Condensed Matter, 2007, 19(16): 165202.

[40] Duck, Ian, and Ennackel Chandy George Sudarshan. "Pauli and the spin-statistics theorem." (1998).

[41] Zeeman,Pieter, and Maxime Bôcher."Zeeman effect." Nature 55.1424 (1897): 347.

[42]Zeeman, Pieter. "XXXII. On the influence of magnetism on the nature of the light emitted by a substance." The London, Edinburgh, and Dublin Philosophical Magazine and Journal of Science 43.262 (1897): 226-239.

[43]Zeeman, Pieter. "VII. Doublets and triplets in the spectrum produced by external magnetic forces." The London, Edinburgh, and Dublin Philosophical Magazine and Journal of Science 44.266 (1897): 55-60.

[44] Guerrero, R., et al. "Shot noise in magnetic tunnel junctions: Evidence for sequential tunneling." Physical review letters 97.26 (2006): 266602.

[45] Governale, M., F. Taddei, and Rosario Fazio. "Pumping spin with electrical fields." Physical Review B 68.15 (2003): 155324.

[46] Chang, A. M., L. N. Pfeiffer, and K. W. West. "Observation of chiral Luttinger behavior in electron tunneling into fractional quantum Hall edges." Physical review letters 77.12 (1996): 2538.

[47] Bychkov, Yu A., and Emmanuel I. Rashba. "Oscillatory effects and the magnetic susceptibility of carriers in inversion layers." Journal of physics C: Solid state physics 17.33 (1984): 6039.

[48] Kovalev, Alexey A., Arne Brataas, and Gerrit EW Bauer. "Spin transfer in diffusive ferromagnet–normal metal systems with spin-flip scattering." Physical Review B 66.22 (2002): 224424.

[49] Crooker, S. A., et al. "Optical spin resonance and transverse spin relaxation in magnetic semiconductor quantum wells." Physical Review B 56.12 (1997): 7574.

[50] Wu, M. W., and C. Z. Ning. "A novel mechanism for spin dephasing due to spin-conserving scatterings." The European Physical Journal B-Condensed Matter and Complex Systems 18.3 (2000): 373-376.

[51] Ney A, Pampuch C, Koch R, et al. Programmable computing with a single magnetoresistive element. Nature, 2003, 425(6957): 485-487.

[52] Behin-Aein B, Datta D, Salahuddin S, et al. Proposal for an all-spin logic device with built-in memory. Nature nanotechnology, 2010, 5(4): 266-270.

[53] Hillebrands, Burkard. Spin dynamics in confined magnetic structures II. Springer, 2003.

[54] Tulapurkar A A, Suzuki Y, Fukushima A, et al. Spin-torque diode effect in magnetic tunnel junctions. Nature, 2005, 438(7066): 339-342.

[55] Busch, G., et al. "Ferro-and metamagnetism of rare earth compounds."Physics Letters 6.1 (1963): 79-80.

[56] McGuire, T. R., et al. "Magnetic properties of some divalent europium compounds." Journal of Applied Physics 34.4 (1963): 1345-1346.

[57] Enz, U., et al. "MAGNETISM OF EuS, EuSe AND EuTe." Philips Res. Rept.17 (1962).

[58]Moruzzi, V. L., and D. T. Teaney. "Specific heat of EuS." Solid State Communications 1.6 (1963): 127-131..

[59] Busch, G., P. Junod, and P. Wachter. "Optical absorption of ferro-and antiferromagnetic europium chalcogenides." Physics Letters 12.1 (1964): 11-12.

[60] Hao, X., J. S. Moodera, and R. Meservey. "Spin-filter effect of ferromagnetic europium sulfide tunnel barriers." Physical Review B 42.13 (1990): 8235.

[61] Busch, G. "Magnetic Properties of Rare Earth Compounds." Journal of Applied Physics 38.3 (1967): 1386-1394.

[62] Stearns, Mary Beth. "Simple explanation of tunneling spin-polarization of Fe, Co, Ni and its alloys." Journal of Magnetism and Magnetic Materials 5.2 (1977): 167-171.] Filip, A. T., et al. "Spin-injection device based on EuS magnetic tunnel barriers." Applied physics letters 81.10 (2002): 1815-1817.

[63] Smits, C. J. P., et al. "Magnetic and structural properties of EuS for magnetic tunnel junction barriers." Journal of applied Physics 95.11 (2004): 7405-7407.

[64] Müller, Norbert, et al. "Electron spin polarization in field emission from EuS-coated tungsten tips." Physical Review Letters 29.25 (1972): 1651.

[65] Kisker, E., et al. "Conduction-Band Tunneling and Electron-Spin Polarization in Field Emission from Magnetically Ordered Europium Sulfide on Tungsten."Physical Review Letters 36.16 (1976): 982.

[66] Moodera, J. S., et al. "Electron-spin polarization in tunnel junctions in zero applied field with ferromagnetic EuS barriers." Physical review letters 61.5 (1988): 637.

[67] Miao, Guo-Xing, and Jagadeesh S. Moodera. "Magnetic tunnel junctions with MgO-EuO composite tunnel barriers." (2012).

[68] Miao, Guo-Xing, Martina Müller, and Jagadeesh S. Moodera. "Magnetoresistance in double spin filter tunnel junctions with nonmagnetic electrodes and its unconventional bias dependence." Physical review letters102.7 (2009): 076601.

[69] Sarid, Dror. "Fowler–Nordheim Tunneling." Exploring Scanning Probe Microscopy with MATHEMATICA, Second Edition: 160-169.

[70] Zhang, X-G., and W. H. Butler. "Large magnetoresistance in bcc Co⁄Mg O⁄Co and Fe Co⁄Mg O⁄Fe Co tunnel junctions." Physical Review B 70.17 (2004): 172407.

[71] Ferreira, R., and G. Bastard. "‘‘Spin’’-flip scattering of holes in semiconductor quantum wells." Physical Review B 43.12 (1991): 9687.

[72] Guinea, F. "Spin-flip scattering in magnetic junctions." Physical Review B58.14 (1998): 9212.